NRC·CNRC

Lab-Based Spectroradiometric Validation of FRL VNIR Imaging Spectrometers

Date: January 6, 2021

Author: Raymond Soffer

Airborne Research Centre,
Flight Research Laboratory

LTR-FRL-2020-0100

National Research Council Canada
Conseil national de recherches Canada

Canada

Paper: Cat. No. NR74-2/2021E
ISBN 978-0-660-37138-2

PDF: Cat. No. NR74-2/2021E -PDF
ISBN 978-0-660-37137-2

Version	Originator	Revision Date	Comments
0.1	Raymond J. Soffer	20-May-20	Preliminary Draft
0.1a	J. Pablo Arroyo-Mora	02-Jun-20	Comments
0.2	Raymond J. Soffer	19-Oct-20	Draft following significant revisions
0.2a	J. Pablo Arroyo-Mora	20-Oct-20	Comments
0.3	Raymond J. Soffer	16-Nov-20	Major revision based upon Pablo's review.
0.4	Raymond J. Soffer	16-Dec-20	Final revision following Pablo's comments
1.0	Raymond J. Soffer	6-Jan-21	Final release pending signatures

Table of contents

Acronyms / Abbreviations 6
1 Introduction 8
2 Background 9
3 Methodology 15
3.1 Calibration of the Integrating Sphere Exit-Port Radiance 15
3.2 Calibration of the HR1024i Portable Spectroradiometer 16
3.3 Integrating Sphere Measurements with Portable Spectroradiometer and HSI. 17
3.3.1 Laboratory Setup 17
3.3.2 Primary Comparison – Absolute Validation Assessment 18
3.3.3 Secondary Comparison – Relative Sensitivity Validation Assessment 19
3.3.4 HSI System Linearity Assessment 21
4 Results and Discussion 22
4.1 Primary Comparison – Absolute Validation Assessment 22
4.2 Secondary Comparison – Relative Radiance Validation 26
4.3 System Linearity Assessment 29
5 Conclusions 36
6 References 38
Appendix A: HR1024i Operational Considerations 39
Appendix B: Hoffman Luminance Standard Sphere Spec Sheet 43
Appendix C: NRC Spectral Radiance Calibration – Hoffman Engineering Spectral Radiance Standard 44
Appendix D: Data Calibration Procedure 54

List of figures

Figure 1. (A) WISE imagery of a location with a deep dark shadow (DDS) used to perform a preliminary assessment of the spectroradiometric calibration of the WISEMan imagery. (B) Radiance spectrum of the DDS with the original spectroradiometric results (Blue), the refined results following in-flight radiometric calibration (IFRC) refinement (ded), and the Modtran5 simulation performed in ATCOR-4 for a target with 0% ground reflectance (green). 14

Figure 2. The integrating sphere observation set up. The HSIs (CASI (shown (G), WISE, µCASI) are interchangeable mounted on platform (E) above the integrating sphere (C) which is mounted in an upward-looking orientation (exit port (D) facing up). The portable spectroradiometer (SVC HR1024i (F)) is mounted on an arm extending off a video tripod similar to our field deployment setup. In this configuration the various radiometric sensors are nadir-viewing, consistent with the orientation in which they are normally deployed on the aircraft or in the field. The integrating sphere is mounted on a lab-jack (B) allowing for the distance between the sphere port and the sensor optics (z-axis) to be manually adjusted in a controlled manner. The lab-jack in turn is mounted on a computer controlled XY translation stages so that positions can quickly and accurately be positioned and reposition between the HSIs and HR1024i (x-axis) or across the FOV (y-axis). 18

Figure 3. Hoffman LS-85-8C Integrating Sphere exit port absolute radiance. (A) Absolute radiance as provided by the NRC Photometry and Radiometry Lab (horizontal orientation) (blue line) in comparison with a derived radiance curve adjusted to a vertical orientation (red line). (B) The spectral relationship between the HR1024i measurements acquired of the sphere exit port radiance in a vertical orientation as compared to in a horizontal orientation with the original data (red line) and 5th order polynomial fit (blue line). 22

Figure 4. (A) Comparison of NRC calibration sphere exit port radiance (horizontal orientation) with that derived from the HR1024i measurements. (B) Repeatability/stability of 12 HR1024i measurements of the sphere exit port radiance (vertical orientation) over the entire HR1024i spectral range. 23

Figure 5. Absolute radiance of the sphere exit port radiance as derived from the spectroradiometrically calibrated (A) WISE, (B) CASI, (C) µCASI (solid green) in comparison with the vertically adjusted NRC calibration results (solid blue) and the HR1024i average results (red solid). The relative differences computed with respect to the NRC calibration (blue dotted) and the HR1024i (red dotted) are plotted on the secondary y-axis. 25

Figure 6. The stepped imagery (red ~ 650 nm, green ~ 550 nm, blue ~ 450 nm) acquired to generate the cross-track statistics are shown for the (A) WISE), (B) CASI, and (C) µCASI. The display look up tables for these images were established using a 2% linear enhancement of the centrally illuminated area. 27

Figure 7. For the (A1) WISE, (B1) CASI, and (C1) µCASI, the absolute spectral radiance mean (solid lines) and CoV (dotted lines) generated for a single column (along-track) (red) and for the multipart ROI covering the entire FOV (cross-track) (blue) are provided. The CoV results for the three instruments are collected into a single chart (D1) to simplify visual comparisons of the results. Corresponding SNR results are provided in (A2) WISE, (B2) CASI, and (C2) µCASI. For the WISE and CASI instruments, the SNR cross-track data prior to spectroradiometric correction is also provide (green). 28

Figure 8. Non-Linearity assessment results for the (A) HR1024i portable spectroradiometer and (B) WISE HSI. Row 1) The radiance data following spectroradiometric calibration for each observed sphere setting. Row 2) The normalized linearity levels for all sphere measurement levels. Row 3) The normalized linearity levels with the lowest integrating sphere settings removed for clarity. 30

Figure 9. . Non-Linearity assessment results are provided for the (A) CASI and (B) µCASI HSIs. Row 1) The radiance data following spectroradiometric calibration for each observed sphere setting. Row 2) The normalized linearity levels for all integrating sphere measurement levels. Row 3) The normalized linearity levels with the lowest integrating sphere settings removed for clarity. 31

Figure 10. Non-Linearity assessment results for an example wavelength of approximately 402 nm with respect to the 100.0% measurements (75% scaled to 100% for the µCASI) for the (A) HR1024i, (B) WISE, (C) CASI and (D) µCASI instruments. The right hand charts (column 1) show the radiance value generated from the original spectroradiometric calibration (L_O) (■) and following a two point calibration refinement (L_C) (▼) compared with that of a perfect linear results (black). The left hand charts (column 2) show the corresponding residual errors for the (L_O) (■) and (L_C) (▲) data. 33

Figure 11. Spectral gains (blue) and offsets (red) as computed within the 2 point calibration refinement process, as defined in **Figure 10,** are provided for the HR1024i (A1), WISE (A2), CASI (A3), and µCASI (A4). The RMS residual error of the originally calibrated radiance data (Lo) (blue) and following calibration refinement (Lc) (blue), defined as the average RMS error with respect to the HR1024i measurement of the integrating sphere set to 100.0%, are provided for the HR1024i (A2), WISE (B2), CASI (C2), and µCASI (D2). Note the different scales used in the HR1024i (A1, A2) charts. 34

List of tables

Table 1: RMS residual statistics extracted from spectral data as shown in **Figure 11** column 2. 34

List of Acronyms / Abbreviations

µCASI. ..... *microCASI*
AC. ..... Atmospheric Correction
ATCOR. ..... Atmospheric and Topographic Correction
BOA. ..... Bottom-of-Atmosphere
cal/val. ..... calibration and validation
CASI. ..... Compact AIrborne Spectrographic Imager
CCD. ..... Charge Coupled Device
CDOM. ..... Coloured Organic Dissolved Matter
CSA. ..... Canadian Space Agency
DC. ..... Dark Current
DDS. ..... Deep Dark Shadow
EO. ..... Electronic Offset, Earth Observation
FOV. ..... Field of View
FPA. ..... Focal Plane Array
FRL. ..... Flight Research Laboratory
FSS. ..... Frame Shift Smear
HSI. ..... HyperSpectral Imager
IFRC. ..... In-Flight Radiometric Calibration
InGaAs. ..... Indium Gallium Arsenide
L1. ..... Level 1 (At Sensor Radiance)
L2. ..... Level 2 (Surface Reflectance)
MODTRAN. ..... MODerate resolution atmospheric TRANsmission
NAP. ..... Non-Algal Particles
NIR. ..... Near InfraRed
NIST. ..... National Institute of Standards and Technology
NRC. ..... National Research Council
SI. ..... International Systems of Units
SL. ..... Scattered Light
SNR. ..... Signal-to-Noise Ratio
SO. ..... Second Order diffracted light
SVC. ..... Spectra Vista Corp.
SWIR. ..... ShortWave InfraRed
TSS. ..... total suspended solids
UAV. ..... Unmanned Aerial Vehicle
UV. ..... UltraViolet
VNIR. ..... Visible and Near InfraRed
WISE. ..... WaterSAT Imaging Spectrometer Experiment

1 Introduction

In 2018, NRC received the WaterSAT Imager Spectrometer Experiment (WISE) instrument from the Canadian Space Agency (CSA) with a request to assess its performance and to make it available to the Canadian remote-sensing community in preparations for the eventual deployment of a Canadian satellite-based hyperspectral instrument dedicated to remote sensing of coastal and inland waters (Qian et al. 2017). The development of the WISE instrument was undertaken as a Technology Readiness Level development task by the CSA to design and test a new, light-weight, small volume, high performance instrument based upon the CASI-1500 heritage with an UV/blue enhanced spectrometer and fore-optics (Qian 2020). With the acquisition of the WISE instrument by the Flight Research Laboratory (FRL) and our associated involvement in remote sensing studies related to coastal and inland waters (WISE-Man – University of Quebec at Rimouski, Lake Erie Western Basin Algal Bloom – University of Waterloo), significant importance is now placed on the UV/blue region of the VNIR Hyperspectral Imager (HSI) sensor data. In the past, airborne HSI acquired by FRL has typically been validated against near-coincidentally acquired ground reflectance measurements of uniform in-scene calibration and validation (cal/val) targets. The acquired at-sensor data, once spectroradiometrically calibrated using lab acquired calibration data, is normally converted to reflectance using the MODTRAN5 Atmospheric Correction (AC) model. When required, the radiometric calibration can be refined by relating the at-sensor radiance levels as derived from inverse application of the AC model to the original radiance results in a process referred to the In-Flight Radiometric Calibration (IFRC) within ATCOR-4. An assessment of at-sensor radiance levels performed with the Compact Airborne Spectrographic Imager (CASI-1500) instrument identified issues with the spectroradiometric calibration of the hyperspectral imagery at wavelengths below 450 nm that will contribute to the challenges in the generation of robust atmospherically corrected imagery (Soffer et al. 2019). As FRL HSI projects previously undertaken did not make use of this portion of the VNIR spectrum, efforts were not made at the time to identify the source of this issue and to identify methods to resolve the issue. Preliminary assessment have indicated that similar issues exist within the UV/blue region of WISE imagery.

This report outlines an effort to produce a quality assessment of the spectroradiometric calibration of the WISE, CASI-1500 and µCASI hyperspectral imaging systems using a lab-based methodology. The absolute accuracy of radiance levels generated following the standard spectroradiometric processing of the HSI imagery of a known, stable and uniform radiance source was initially assessed. Secondly, the ability to correct for variations in the pixel sensitivities across the entire HSI field of view was evaluated in terms of noise and the resulting signal to noise levels. As these evaluations are normally performed at a single spectral radiance level, the linearity of the systems were evaluated over a wide range of input radiance levels typical of those encountered in earth observation airborne HSI data sets. Finally, the effectiveness of a standard approach used to correct errors in the absolute spectroradiometric calibration of earth observation HSI imagery was assessed.

2 Background

Inland and coastal waters are, in general, optically complex, and often optically shallow, i.e. where the light reflected by the bottom makes a significant contribution to the water-leaving signal (IOCCG 2000). Given the significant absorption that occurs within a water column in the red and near infrared (NIR) portion of the electromagnetic spectrum, the relevance of light interactions in the upper ultraviolet (UV) through green spectral region is of increased importance in earth observation (EO) remote sensing applications that seek to characterize bottom structures (bathymetry, vegetation beds) or determine water column quality via optical properties (phytoplankton), non-algal particles (NAP), coloured organic dissolve matter (CDOM), detritus, total suspended solids (TSS)) (Ogashawara et al. 2017). This contrasts with terrestrial applications in which surface reflected energy in the green through NIR portion of the VNIR spectral region often dominate multi and hyperspectral analysis techniques. This is due in part to challenges encountered in the UV/blue related to the acquisition and calibration of remote sensing data sets of adequate quality in terms of absolute at-sensor radiance. This spectral region is subject to relatively poor sensitivity levels in typical of state-of-the-art solid state detector systems. This is compounded by challenges in the conversion of such data to surface reflectance through the application of atmospheric correction (AC) models which are heavily impacted by atmospheric scattering at these wavelengths.

Significant efforts have been undertaken at NRC-FRL to validate reflectance (Level-2 - L2) data products produced from our airborne and Unmanned Aerial Vehicle (UAV) hyperspectral imagery making use of field spectrometry (cal/val) measurements (Arroyo-Mora et al. 2019; Arroyo-Mora et al. 2018; Kalacska et al. 2016; Soffer et al. 2019). These efforts included the development and assessment of field spectroscopy methodologies including quality assessment techniques and the calibration of the field reference panels used as the underpinnings to produce high quality field reflectance measurements (Soffer et al. 20191). In this process, imagery that has been spectroradiometrically calibrated to units of spectral radiance (Level 1 – L1) using laboratory acquired calibration data is converted to a reflectance data product making use of an AC model prior to the validation process (ATCOR-4) (Richter and Schläpfer 2019). The ATCOR-4 modelling process, which is based upon MODTRAN5 AC code, requires numerous parameters be entered to model the transmission of the radiance through the atmosphere (downwelling, upwelling, and in-scattered) and the instrument response itself.

In addition to potential errors in the absolute sensor spectroradiometric calibration data and processing (ITRES Research Ltd. 2017), discrepancies between the resulting L2 results and the “ground truth” reflectance can also be due to 1) inaccuracies in the determined ground truth (contamination in downwelling irradiance due to local in-scattering surfaces, fluctuation in the downwelling irradiance due to changing atmospheric conditions (aerosols, H_2O, clouds etc.), or 2) errors in the application of the AC model. In the work presented by Soffer et al. 2019, the CASI-1500 L2 comparisons indicate that although the reflectance levels derived in this fashion

from the airborne results strongly resembled that of a number of cal/val targets (asphalt, concrete, grey tarp, black tarp) between 450 nm and 1050 nm, a discrepancy of increasing magnitude occurred at wavelengths less than 450 nm (down to 375 nm in the CASI-1500). Since previous research interests at FRL made use of wavelengths greater than 450 nm, the issue with the reflectance data quality below 450 nm was noted but no significant effort was spent on understanding the source of the error and its rectification. With the acquisition of the WISE instrument and its interest in aquatic applications, accuracy of spectral results below 450 nm are now critical due to its importance in such work (Ogashawara et al. 2017).

Multiple issues related to the generation of reliable reflectance imagery derived from VNIR HSI in the UV/blue spectral regions are known to be of concern. First, the ability to accurately spectroradiometrically calibrate the instrument in this spectral region is noted. Silicon-based sensors typically used in VNIR hyperspectral systems have inherently poor response to incident photons at either end of the spectral region (i.e., < 450 nm, > 900 nm) (Janesick 2001) resulting in low signal response with extreme susceptibility to small errors in the data conditioning (electronic offset (EO), dark current (DC), scattered light (SL), frame shift smear (FSS), second order diffracted light (SO)). Secondly, the optical design of the spectrometer for these 'VNIR' systems typically compound this issue as the design tends to be optimized for the central region of the spectral range (~700 nm). Of primary concern here is the blazing wavelength for which the diffraction grating is designed and optimized. For the WISE instrument the grating and the entire optical system was 'blue shifted' in its design in order to improve the spectroradiometric response in the UV/blue spectral region critical to aquatic applications. Finally, this poor responsivity is compounded by significantly decreased radiance levels in most in-lab calibration sources. Blue enhanced sources are available but they tend to introduce problems in the UV/blue portion of the spectrum, specifically sharp spectral features, which make them less suitable for use as a spectroradiometric calibration source (D'Amato 1998). The calibration challenges of hyperspectral data in the UV are further compounded by the relatively low bottom-of-atmosphere (BOA) downwelling irradiance levels in this spectral region (Slater 1980). It has been noted that over blue ocean waters atmospheric contributions dominate the overall observed at-sensor radiance levels with only ~10% coming from the target of interest, the water column (Ilori et al. 2019). Although the radiance exiting shallow and optically complex typical of coastal and inland waters are likely to be more significant than those of blue ocean waters, even a small discrepancy in the estimated atmospheric contributions to the observed at-sensor radiance levels, including that of path radiance, will have a profound impact on the AC process.

The initial absolute spectroradiometric calibration of the three HSI instruments was performed by the instrument manufacturer using a Labsphere Luminance Radiance Source (formally SphereOptics) (ITRES Research Ltd. 2010). The sphere is equipped with port reducer (slit) designed to increase the sphere efficiency and output uniformity which is increasingly challenging to maintain with larger sphere and larger exit ports. This sphere is in turn calibrated by Labsphere which is traceable to SI units though the NIST radiance standard. According to

the instrument manufacturer and calibrator, the uncertainty of the integrating sphere used to perform the calibration of the HSI instruments under evaluation in this study is ±2.0% (private communication, ITRES Research 2020). No indication has been provided with respect to the increase in uncertainty following transfer to the HSI instrumentation.

It is assumed that errors in the estimation and application of suitable offsets values applied in the data conditioning, even if miniscule in the regions of poor input radiance and system responsivity, may lead to significant errors in the absolute radiance determined following radiometric scaling. It is conceivable that such errors may appear as a non-linearity that are negligible for high signal levels and most noticeable for low signals, similar to what has been observed. The methodology used in the calibration of the HSI equipment uses a single point calibration approach. Such an approach makes the assumption that the calibration curves which are generated for each pixel, passes linearly between the calibration point and the origin but only after any offset contributions have been precisely removed. In other words, if an input radiance level of zero is observed on a given detector pixel following the removal of offset contributions, an output of 0 digital numbers (DNs) would be expected. The offsets, as previously listed, include a SO correction to reject second order scattered light. In the CASI-1500 and µCASI a model is used estimate the SO contribution that is applied in the data conditioning. The WISE instrument incorporates a physical filter to reject SO from the diffraction grating and is therefore is not addressed in its calibration process. For the µCASI, whose design is based upon a focal plane array (FPA), FSS is not an issue in the readout process and the physical structure used in the charge coupled device (CCD)-based system to estimate the SL is not available. Through the acquisition and analysis of a suitable lab-based dataset, the instrument manufacturer carried out a system characterization with a test known as a photon (or light) transfer curve analysis (Janesick 2001), and has indicated that there is no concern with the linearity of the system. This process, however, looks at the raw data prior to offset correction and radiometric scaling so would not reflect a non-linearity should it be introduced by the calibration procedure itself. Given the sensitivity issues, as discussed earlier, in the UV/blue spectral region of these instrument, minute errors in the offset estimations are capable of introducing significant errors in the radiometric calibration process. This concern applies to not only the processing of the remotely sensed image but also to that of the calibration data set itself. An examination of a sample dataset can provide a clear illustration of the potential issue. A spectral radiance of 1.0 µW/cm²/sr/nm at 393 nm, acquired at a typical integration time of 50 ms, would generate a radiance induced value of approximately 100 DN. The combined offset applied to this pixel was identified to be 900 DN. An error in the combined offset of only 10 DN would therefore result in an error of 10%.

The ATCOR-4 IFRC approach is typically implemented as a two-point calibration approach to refine the original spectroradiometric calibration results. Based upon ground reflectance levels, two radiometrically distinct surfaces with known ground reflectance levels are identified and used to correct for residual errors in the derived image at-sensor radiance levels (Richter and

Schläpfer 2019). This approach also assumes system linearity but does not necessarily assume that the calibration curve extend through the origin. Evaluation of results determined when attempting to refine the calibration through this methodology has suggested that non-linearity's in the spectroradiometrically calibrated data may in fact provide a possible explanation for the observed errors in the calibration results typical of low signal levels in the UV/blue. With this in mind, despite the fact that the instrument manufacture's laboratory tests suggest a linear system, an independent test of the system linearity following calibration is necessary.

Following acquisition of HSI imagery for the WISE-Man campaign in August 2019, sample spectroradiometrically calibrated imagery (L1A), including that of an image of a land-based cal/val site in support of the WISE-Man 2019 project was assessed. A preliminary assessment of the spectroradiometric calibration was carried out and issues of concern were identified. The reflectance of the three cal/val targets within the imagery (black tarp, asphalt, grey tarp) following AC with ATCOR-4 were compared with those determined using near-coincidental field spectroscopy measurements acquired as described in Soffer et al. (2019). Significant errors were apparent over most of the spectral range when the comparative spectra were visually compared. Following application of the IFRC refinement process applied using any two of the three cal/val targets (the third target is retained for use as a validation point) the generated surface reflectance spectra closely resembled the in situ results over much of the spectral region. Despite the fact that the black tarp had a reflectance value of between 3% and 4%, validation of even darker targets appeared to be required. This is necessary in order to understand why the reflectance levels of dark pixels derived within the HSI imagery, such as shadows and water, as well as the UV/blue spectral region of even much brighter pixels, were significantly lower than expected. Since ground validation data was not acquired of such dark targets, other approaches, albeit less accurate, had to be identified to assess the quality of those dark pixels. The reflectance of a deep dark shadow (DDS) pixel from within the WISE-Man cal/val image was examined (**Figure 1A**) for this purpose. Evaluation of the IFRC generated reflectance of the DDS revealed ground reflectance levels that were negative over much of the spectral range. In order to assess this result, the at-radiance spectra for these pixels were examined following the original calibration (L_O) as well as following IFRC correction (L_C) prior to correction to reflectance. For the DDS pixel, it was assumed that the downwelling direct irradiance incident on the ground surface is negligible which would generate an at-sensor radiance result as if the ground reflectance of the pixel was equal to 0%. The at-sensor radiance levels would in such a case be comprised entirely from path radiance L_P (Arroyo-Mora et al. Under Review). Inverse execution of the AC model applied using a ground reflectance level at 0% would therefore provide an estimate of the at-sensor radiance levels for the DDS pixel. **Figure 1B** shows significant overestimation of L_O over most of the spectral range and significant underestimation of L_C with respect to the anticipated path radiance L_P as generated by the MODTRAN5 AC model implemented within ATCOR-4 for a ground reflectance equal to 0% with other parameters set to match the WISE instrument and the flight conditions. Although it is

noted that the shape of the L_O follows that of L_P over much of the spectral range, any correlation appears to disappear for wavelengths less than 420 nm.

These preliminary findings suggest two possibilities. First, the significant correction that is determined by the IFRC process that results in the generation of reasonable reflectance spectra for the three cal/val targets indicate that there is a radiometric calibration error of significance in the WISE instrument that appears to be, or at least close to, linear in nature for pixels with significant signal levels. Secondly, when low signal levels are encountered, that linear correction appears to be overcorrecting the radiance values resulting in negative radiance suggesting. Such a result suggests a non-linear radiometric correction for low signal levels. It is essential that the source of this issue be understood and rectified in order to reliable perform any analysis of the data that make use of pixels subject to weak spectroradiometric signals. The assumption here hasn't characterized the signal-to-noise ratio (SNR) to evaluate if the instrument has the required SNR for low albedo targets (e.g., shadow and water pixels) (Arroyo-Mora et al. Under Review).

Although the work described here was initiated to better understand possible calibration issues identified within the WISE imagery acquired for the WISE-Man project dataset, the experiment ultimately was designed and performed to evaluate the spectroradiometric calibration accuracy of the entire suite of VNIR imaging spectrometers operated by FRL. The process is equally applicable to the SASI imager as well but as yet not been carried out. Three separate data sets were acquired of an illumination source of know spectral radiance with each of the three VNIR imaging spectrometers, the WISE (SN: 2606), CASI-1500 (SN: 2511), and µCASI (SN: 6501). First HSI measurements were acquired of a recently calibrated integrating sphere to assess the absolute spectroradiometric calibration accuracy. A second data set was acquired in which the integrating sphere exit-port is viewed across the entire HSI field of view (FOV) so the effectiveness of the spectroradiometric calibration could be assessed as a function of spatial pixel (column) of the imager. A third data set was acquired at various sphere intensity levels in order to assess the system linearity across a wide range of input radiance levels.

The processes applied to the HSI instrument data acquired and assessed in this study have not previously been validated. With its simpler structure, the Spectra Vista Corp. (SVC) HR1024i portable spot (non-imaging) spectroradiometer results are therefore viewed as being of significant importance within this study, providing significant insights into the capabilities of the implemented experimental procedure. Unlike the spectroradiometric calibration of the integrating sphere that was performed using a transfer radiometer in an entirely different physical configuration (orientation) and environment, the HR1024i radiance measurements of the sphere were acquired in a configuration (vertically orientation) and physical environment identical to those performed with the three HSI systems. Previous work performed with the HR1024i had provided significant insights into the stability impacting the accuracy and precision of the system performance (i.e., temperature and integration time instabilities) that are critical to

the successful acquisition of the data sets required in this effort and their interpretation. As these have yet to be published, they have been summarized in **Appendix A.**

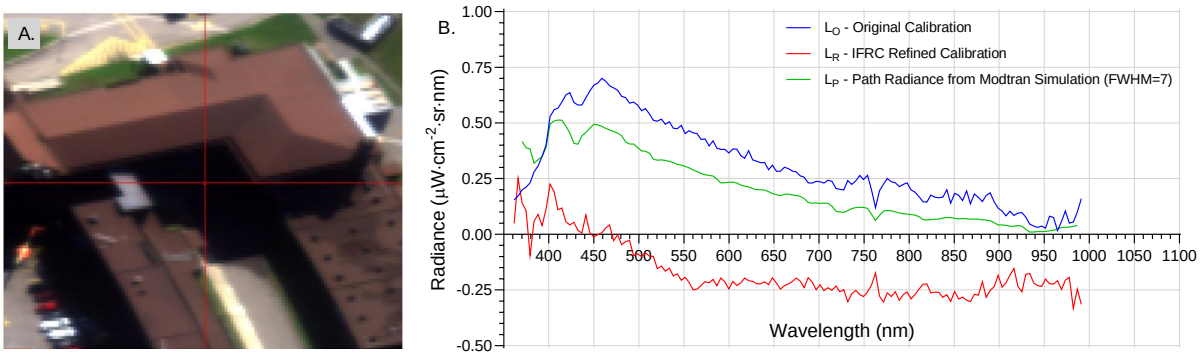

Figure 1. (A) WISE imagery of a location with a deep dark shadow (DDS) used to perform a preliminary assessment of the spectroradiometric calibration of the WISEMan imagery. (B) Radiance spectrum of the DDS with the original spectroradiometric results (Blue), the refined results following in-flight radiometric calibration (IFRC) refinement (Red), and the Modtran5 simulation performed in ATCOR-4 for a target with 0% ground reflectance (Green).

3 Methodology

The procedures described here not only relate to those performed to assess the validation of the spectroradiometric performance of the HSIs but also to outline the external procedures used to prepare the supplemental equipment, specifically the integrating sphere and portable spectroradiometer, with which this laboratory work was performed.

3.1 Calibration of the Integrating Sphere Exit-Port Radiance

In order to assess the absolute accuracy of the spectroradiometrically corrected data of our three VNIR imaging spectrometers, a stable source of known radiance levels was required. A Hoffman LS-65-8C Luminance Standard Sphere (**Appendix B**) (hereafter referred to as the 'integrating sphere' or simply 'sphere') suitable for this task was available. This source had been used in previous assessments and significant confidence had been established based upon those results in the short term stability (periods of seconds to hours), repeatability, linearity, and uniformity of the radiometric output of the sphere (Soffer, unpublished). The output radiance level of the integrating sphere is controlled by a curved Vernier slit caliper used to control the input light levels to provide a known value as provided by a photopically corrected silicon detector monitor incorporated as part of the integrating sphere instrument control unit. The curved slit design of the Vernier allows for the precision with which the adjustment of the aperture size, and therefore input radiance levels, is controlled to increase with decreasing size. Concern existed that the interior of the Barium Sulphate ($BaSO_4$) coated sphere or the quartz halogen bulb used as the illumination source, could have been subject to spectrally dependent deteriorations resulting in changes to the spectral radiance output of the exit port over time. As the absolute spectral radiance of the sphere had not been calibrated since 1993, it was therefore important that the sphere be re-calibrated to account for these potential issues.

The integrating sphere was sent to the NRC Photometry and Radiometry Lab, custodians of the Canadian radiometric standard, to have the current spectral radiometric output of the sphere exit-port calibrated with the monitoring photodiode set to 100.0%. The sphere calibration was performed using a transfer radiometer (Photo-Research PR-715 Spectroradiometer) between 380 nm and 1068 nm at 2 nm spectral sampling intervals. This transfer radiometer is in turn calibrated using a lamp/reflectance standard prepared according to, and traceable with respect to, National Institute of Standards and Technology (NIST) protocols. The traceability to SI units is through an international comparison of irradiance lamp standards for wavelengths between 300 nm and 690 nm as well as through measurements using the NRC absolute radiometer between 700 nm and 1600 nm.

Although it was known that the sphere would be used in a vertical orientation (exit port pointing in a vertical, upwards looking, direction), the configuration of the NRC calibration could only be implemented with the sphere in a horizontal orientation (exit port pointing in a horizontal

direction). In order to ensure that the integrating sphere remains operationally stable, the Vernier and power setting of the integrating sphere required to provide a 100.0% output reading during the lab use of the sphere were noted and compared against those noted during the calibration process.

3.2 Calibration of the HR1024i Portable Spectroradiometer

The Spectra Vista Corp (SVC) HR1024i portable spectroradiometer (SN: 2047) (SVC 2019) was acquired by the FRL in 2011. Since then, measurements obtained with the instrument have been used as the baseline for airborne and UAV cal/val work performed by FRL (Soffer et al. 2019). The HR1024i spectroradiometer covers the spectral range from 340 nm to 2550 nm. The incoming radiation, introduced into the system through an interchangeable fore-optics (a 4° FOV fore-optic is used in this work), is divided between three spectrometers. The first covering the VNIR spectral range (340 nm to 1023 nm) with a linear silicon CCD array detector, the second covering the SWIR1 spectral range (971 nm to 1900 nm) using a single element, temperature controlled, Indium gallium arsenide (InGaAs) detector, and the third covering the SWIR2 spectral range (1900 nm to 2500 nm) also using a single element, temperature controlled, InGaAs detector.

In addition to the field work, the instrument has been used to perform precise laboratory directional reflectance measurements of the reference panels used in the field work (Soffer et al.). The expertise developed in these efforts, both in the field and in the lab, was developed using the instrument to perform relative measurements acquired over relatively short periods of time (seconds to a few minutes). Such work either sought to determine a surface's reflectance through comparative measurements with a panel of know reflectance or attempted to determine uniformity of a surface through comparison of multiple measurements. Although the lessons learned in the application of such work are applicable to the acquisition of the robust measurements require in this current work, absolute spectroradiometric calibration of this instrument has not been maintained on a regular basis with two years of lab and field campaigns since it was last calibrated.

The spectroradiometer was therefore sent for recalibration by instrument manufacturer immediately prior to the data acquisition performed in this work in order to assess our ability to compare absolute spectroradiometric results of a recently calibrated instrument with those expected. The HR1024i calibration was performed using an Optronics Laboratory OL 455-12SA-2 Integrating Sphere which was in turn calibrated by Optronics Laboratory "relative to standards supplied by the National Institute for Science and Technology". The uncertainty of the OL 455-12SA-2 was stated as < ±2% relative to the NIST photometric scale. The total uncertainty of the HR1024i calibration will also include a contribution from the transfer process from the sphere to the radiometer that are not provided with this calibration.

3.3 Integrating Sphere Measurements with Portable Spectroradiometer and HSI.

3.3.1 Laboratory Setup

The setup within the FRL dark room for the acquisition of the imaging and portable spectroradiometer measurements of the integrating sphere is depicted in **Figure 2**. The setup was configured so that the spectroradiometers were in a nadir (downward) viewing orientation in order to operate the sensors in their normal orientation. The integration of the computer controlled XY translation stages as well as the manually controlled lab-jack (z-axis) provided assistance with determining the optimal initial positioning of the sphere within the FOV of the portable spectroradiometer and HSI instruments with the ability to precisely reposition it at a later time. The spectroradiometer was outfitted with a 4° FOV fore-optic for all measurements. With a nominal lens-to-port separation distance of 17.0 cm, the size of the spot being viewed at the sphere exit port will be 1.0 cm, well within its 4.0 cm diameter. The assertion that the FOV fit cleanly within the integrating sphere exit port (without edge effects) was verified by a series of measurements made with the lens-to-port separation distance varied between 10.0 cm and 43.0 cm to ensure that the spectroradiometer measurements remain consistent (< 0.1% variation) at all tested separation distances. Similar comparative measurements were performed with the sphere translated over a range of ±1 cm from the identified central location in the x and y-axis to similarly ensure that the measured radiance levels remained unaffected by the exact location being viewed within the integrating sphere exit port. With a nominal FOV of 40° for the CASI-1500 (hereafter referred to simple as the CASI) and WISE and 34.4° for the µCASI, the exit port of the integrating sphere filled only a small portion of the entire imager FOV. As such separate measurement scenarios were required to acquired data to perform an 1) absolute validation assessment and 2) a relative sensitivity validation assessment (uniformity or flat field correction). A third scenario is provided to acquire a data set to assess the linearity of spectroradiometrically calibrated data. The lab procedures are provided in **Appendix D**. The entire process was performed first for the portable spectroradiometer and then repeated for each of the 3 imaging spectrometers. Included in the procedure is an additional absolute radiance check made with the HR1024i immediately prior to and immediately following the data measurement sequence performed with each HSI in order to confirm the radiometric stability/repeatability of the integrating sphere output over the duration of, and between, each data acquisition sequence.

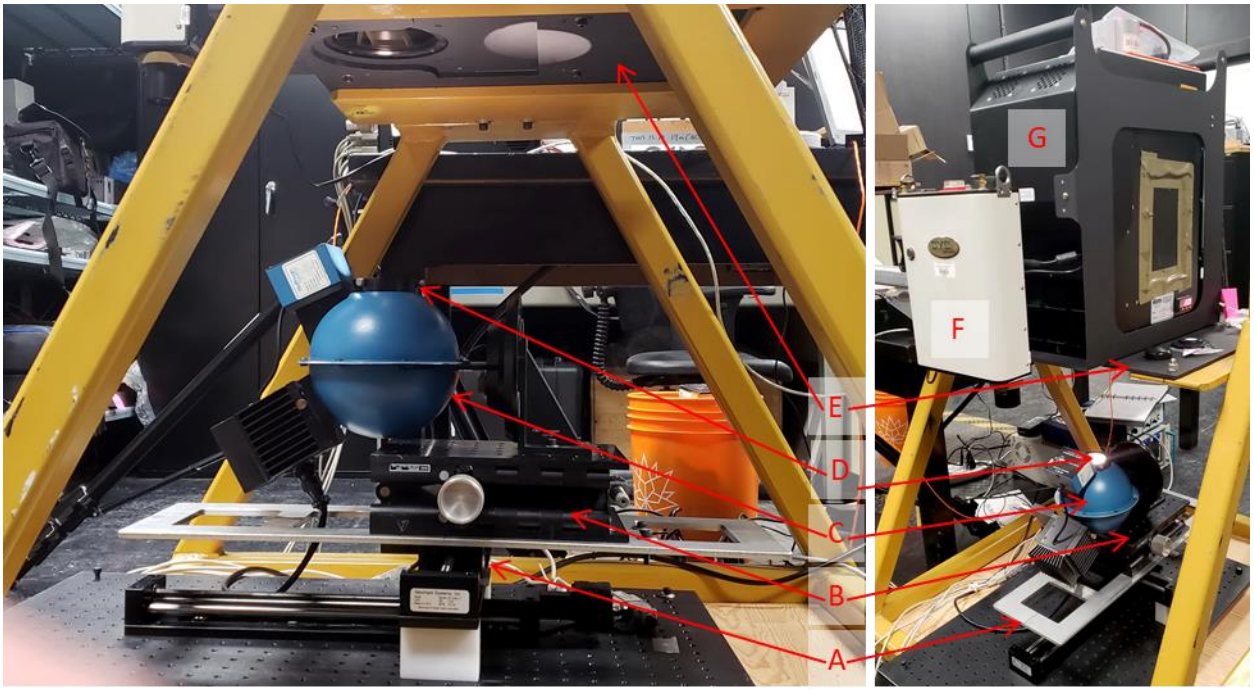

Figure 2. The integrating sphere observation set up. The HSIs (CASI (shown (G), WISE, µCASI) are interchangeable mounted on platform (E) above the integrating sphere (C) which is mounted in an upward-looking orientation (exit port (D) facing up). The portable spectroradiometer (SVC HR1024i (F)) is mounted on an arm extending off a video tripod similar to our field deployment setup. In this configuration the various radiometric sensors are nadir-viewing, consistent with the orientation in which they are normally deployed on the aircraft or in the field. The integrating sphere is mounted on a lab-jack (B) allowing for the distance between the sphere port and the sensor optics (z-axis) to be manually adjusted in a controlled manner. The lab-jack in turn is mounted on a computer controlled XY translation stages so that positions can quickly and accurately be positioned and reposition between the HSIs and HR1024i (x-axis) or across the FOV (y-axis).

3.3.2 Primary Comparison – Absolute Validation Assessment

The primary measurement was designed to validate the HSI instrument spectroradiometric calibration at a single pixel located centrally within the FOV. Care was taken to ensure that the image slit was viewing the sphere exit port close to its central position in the along-track (x-axis) direction by ensuring that location produce a maximized port image width. As previously noted, the integrating sphere calibration by NRC's Photometry and Radiometry Lab was performed in a horizontal orientation to accommodate their calibration configuration. To evaluate whether the radiometric output of the sphere exit port varies as a function of its system orientation, an additional measurement was performed in the FRL dark room of the sphere in a horizontal orientation using the HR1024i to assess the stability, and if necessary, to account for variability in the sphere radiometric output due to its orientation.

The spline function within Matlab was used to resample to the spectra of the resulting data sets to a common wavelength grid, that of the HR1024i, in order to allow the absolute radiance levels to be quantitatively compared with that of the NRC calibration. A graphical comparison was performed of each of the resampled data sets against the original data ensured that no unexpected spectral features were introduced into the resampled data (results not provided).

With the acknowledged temperature sensitivity of the HR1024i VNIR detector (**Appendix A)**, adequate time was provided to allow the system to stabilize to the temperature at which the HR1024i calibration was performed.

3.3.3 Secondary Comparison – Relative Sensitivity Validation Assessment

Earlier investigations performed with CASI airborne data sets assessing the quality of the derived reflectance levels suggested that the reduction in the radiometric accuracy at the blue end of the spectrum may increase in significance near the edges of the FOV (Soffer et al. 2019). This data set seeks to quantify the quality of the calibration data set/process to perform uniformity corrections across the entire FOV of the HSI under test by comparing the noise (as a function of wavelength/channel) generated across a simulated flat field against that which would be generated from a perfect uniformity correction. The noise determined as a function of each spectral channel in the along-track results will have been determined for a single pixel. Noise levels will therefore have originated from the system read noise and shot noise, common to all pixels, with zero contributions due to pixel-to-pixel sensitivity issues (assuming the responsivity remains stable throughout the period of data acquisition) or variation in the radiometric input (assuming stability of the radiometric input). Assuming input radiance field across the entire instrument FOV, increases in the noise levels derived in the cross-track data with respect to the baseline (along-track) nose levels will be attributable to less than perfect compensation for pixel-to-pixel sensitivity variations to photons incident on the system.

Assuming that the input radiance and responsivity of an individual pixel (i.e., that examined in the primary comparison) remains unchanged over the data acquisition period, the baseline noise levels (that attainable if perfect uniformity correction is achieve) can be estimated as that derived from multiple scan lines (integration periods) of that individual pixel.

Ideally a data sets of a horizontally uniform source that covered the entire HSI FOV would be used to acquire the necessary data. This would normally be accomplished using a large integrating sphere (500 mm diameter) with a large exit port (20 cm wide) as is implemented by the instrument manufacturer when performing calibration procedures. Such systems are costly to purchase and the larger the sphere/exit port, the greater the challenge in maintaining radiometric uniformity across the exit port. As such a system was not at our disposal, a simulated flat field data set is produced with the 150 mm diameter Hoffman LS-65-8C Luminance Standard Sphere by ‘stepping’ the integrating sphere exit port (40 mm) across the HSI FOV using the translations stage upon which it is mounted. Each step is made with significant overlap in the exit port image with that of the adjacent step in order to avoid edge effects. A single row region of interest (ROI) (one pixel per column – 1500 columns) is then assembled from the pixels centrally located within the exit port image of each ‘step’. In order to provide coverage to the edges of the FOV using the translation stage, it was necessary to reduce the lens-to-port distance to 14.0 cm from that used for the absolute calibration assessment (17.0 cm). This was accomplished making use of the vertical adjustment on the lab-

jack platform upon which the sphere was mounted. The monitoring photodiode response for these measurements was maintained at 100.0% throughout this measurements sequences.

With the significant variability in the radiance levels as a function of wavelength, the results are more easily compared when displayed as the coefficient of variation (standard deviation/mean) (CoV). The equation for the baseline situation (single spatial pixel), for each spectral channel, is therefore defined as:

$$CoV_{AT} = \frac{\sigma_{AT}}{\mu_{AT}} = \frac{\sqrt{\frac{\sum_{sl=1}^{sl=N_{SL}}(x_{sl} - \mu)^2}{N_{SL}}}}{\mu_{AT}}$$

where AT refers to the 'along track' results, sl is the scan line number from 1 to N_{SL}, x_{sl} is the radiance value for pixel sl, and σ_{AT} and μ_{AT} is the standard deviation and mean signal computed over the N_{SL} scan lines. For the cross tract full FOV results (1 pixel per spatial location), the CoV is defined as:

$$CoV_{XT} = \frac{\sigma_{XT}}{\mu_{XT}} = \frac{\sqrt{\frac{\sum_{p=1}^{p=N_P}(x_p - \mu)^2}{N_P}}}{\mu_{XT}}$$

where XT refers to the 'cross track' results, p is the pixel number from 1 to N_P where N_P = 1500 for the WISE, 1496 for the CASI, and 1865 for the µCASI, x_p is the radiance for pixel p, and σ_{XT} and μ_{XT} is the standard deviation and mean signal computed over the N_P pixels.

It is also useful to examine this results when inverted to be viewed as the Signal to Noise Ratio (SNR = 1 / CoV). As an assessment of the impact of the uniformity correction itself, the SNR is also determined for the WISE and CASI prior to the spectroradiometric correction but following the offset correction.

SNR is a specification of primary concern to end users for Earth Observation HSI data. The theoretical SNR that is often provided as a system specification describing the capability of a HSI system is commonly determined from system noise floor and gain levels. In practice, this will result in SNR levels comparable to those generated from the along-track data (SNR_{AT} = 1 / CoV_{AT}) for the radiance levels as provided by the integrating sphere set to 100.0%. Comparison of SNR levels generated from the cross-track data (SNR_{XT} = 1 / CoV_{XT}) with respect to SNR_{AT} provides an opportunity to investigate the impact of the uniformity correction process on the resulting SNR levels. In practice, a real data set is likely to include a combination of both cross-track pixels and along-track scan lines resulting in a spectral SNR curve that is likely to fall somewhere between these cases.

3.3.4 HSI System Linearity Assessment

The system linearity assessment methodology takes advantage of the inherent stability and linearity of the Hoffman Integrating Sphere and it's built in monitoring photodiode. The monitoring photodiode built into the sphere wall provides feedback, in terms of its spectrally broad photonic response, to be monitored and adjusted to precise relative radiometric levels. The exit port output radiance levels are continuous controlled through the adjustment of the curved Vernier slit through which the light enters the sphere. Such an approach ensures radiance adjustments are made with a single bulb operated at a constant current level with the supplied precision power supply. This ensures that the colour temperature of the filament, and therefore the spectral radiometric output of the bulb remains consistent.

Prior to application of the system linearity test to the HSIs, the linearity of the integrating sphere radiometric output as a function of wavelength was assessed using the HR1024i. With the equipment configured as described for the absolute validation assessment, measurements were acquired with the sphere output radiance adjusted to numerous levels between 130.0% and 0.005%. The exact reported levels were recorded and visually monitored to ensure that the reported level remain constant during the each data acquisition period. This process was repeated for the three HSI instruments with the sphere positioned centrally within the instrument FOV. The integrating sphere control unit has a precision setting that increases the precision of the photodiode readout as the radiance levels decreases. It is important that the sphere output be set and recorded using the maximum precision possible for the radiance level being used (1 digit of precision for the brighter sphere levels (i.e., > 70%), 2 for the moderate settings (i.e., 20.00% to 70.00%), and 3 for the low levels (i.e., < 20.000%)).

The linearity of the systems were assessed by dividing the radiance levels derived from the data acquired at the various sphere output settings against that derived from the 100.0% measurement. A perfectly linear system would therefore provide a value equal to the ratio of the recorded sphere output i.e. 50.00% / 100.0% = 0.50. In order to simplify viewing the spectral curves at all levels, the results were then normalized against the anticipated value which would then results in a value of 1.000 for a perfectly linear result.

4 Results and Discussion

4.1 Primary Comparison – Absolute Validation Assessment

The integrating sphere exit port radiance calibration was performed by the NRC Photometry and Radiometry Lab on February 5 and 6th, 2020. Additional details of the calibration process are provided in the calibration report (**Appendix C**). The final calibration results provided were an average of the results obtained on the two days (**Figure 3A -** blue line) with the setup being entirely reconstructed each day. As previously noted, due to limitations in the positioning of the NRC Photometry and Radiometry Lab's radiance calibration system, the sphere calibration was performed in a horizontal orientation rather than the vertical orientation that is necessary when using it as an absolute radiance source with the HSI equipment. An assessment was therefore performed to quantify the changes making use of HR1024i measurements of the sphere exit port made in both orientations with the monitoring photo diode set to 100.0% in each. The resulting spectrally dependent relationship (**Figure 3B -** red line) was fit with a 5th order polynomial fit (**Figure 3B -** blue line) in order to ensure that the noise contributions evident at either end of the spectral range are not introduced when the results were used to modify the calibrated horizontal absolute spectral radiance to derive the expected vertical absolute spectral radiance (**Figure 3A** – red line). The spectral nature of the variations, which ranged from +3.0% (350 nm) to -1.3% (1050 nm), suggests that the changes are due to a variations in output of the

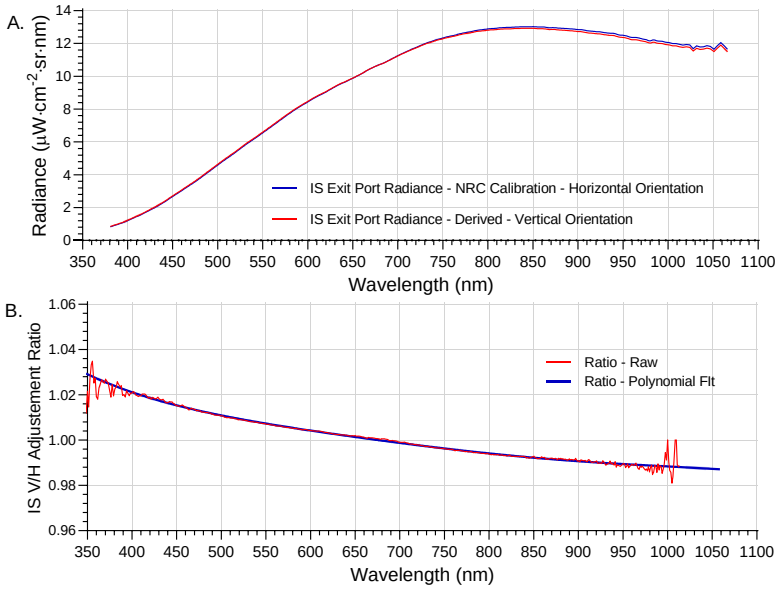

Figure 3. Hoffman LS-85-8C Integrating Sphere exit port absolute radiance. (A) Absolute radiance as provided by the NRC Photometry and Radiometry Lab (horizontal orientation) (blue line) in comparison with a derived radiance curve adjusted to a vertical orientation (red line). (B) The spectral relationship between the HR1024i measurements acquired of the sphere exit port radiance in a vertical orientation as compared to in a horizontal orientation with the original data (red line) and 5th order polynomial fit (blue line).

bulb/filament itself rather than a change in the amount of light entering the sphere through the Vernier slit. This approach assumes that the HR1024i is insensitive to orientation effects, something that is unproven at this time.

Calibration of the HR1024i portable spectroradiometer with the 4° FOV fore-optics was performed by SVC on February 5th, 2020. Both the absolute radiance and wavelength calibration were performed at a reported VNIR detector temperature of 36.6°C. Since no adjustments were performed to the HR1024i instrument optical, detector, and detector readout electronics during the 2020 calibration effort that would impact the system performance, a direct comparison was performed of those results with that of the previous calibration (February 9th, 2018) in order to comment on the long-term stability of the instrument. Wavelength registration variations within the VNIR portion of the system were limited to 0.0 to +0.3 nm and relative changes to the radiometric sensitivity were found to be between 4.2% and -2.5% in the VNIR. Despite having been involved in numerous field and lab measurement campaigns in the period between calibrations, these relatively small changes in the system response are not suggestive of long-term stability issues within the system.

The absolute radiance derived from the HR1024i measurements of the sphere exit port radiance are compared with those determined in the NRC calibration (**Figure 4A)**, with both acquired in a horizontal orientation. Although the relative difference between 450 nm and 670 nm align to within ±2%, the discrepancy varies from +3.5% (400 nm to 440 nm) and to -12.5% (975 nm).

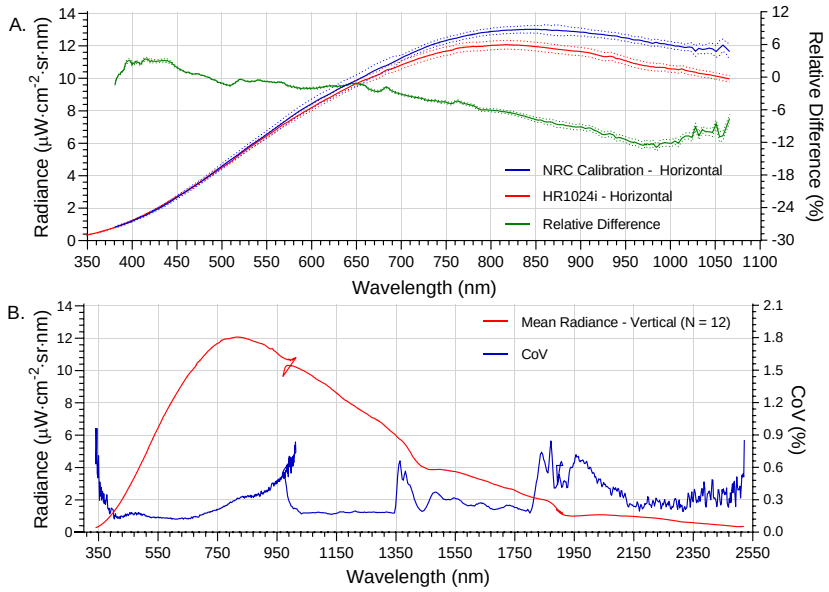

Figure 4. (A) Comparison of NRC calibration sphere exit port radiance (horizontal orientation) with that derived from the HR1024i measurements. (B) Repeatability/stability of 12 HR1024i measurements of the sphere exit port radiance (vertical orientation) over the entire HR1024i spectral range.

The NRC sphere calibration results are provided with the expanded uncertainty (k=2) as provided in the calibration report. As the complete uncertainty was not delivered with the HR1024i derived radiance levels, a 'best case' uncertainty is included with its results. The stated known 2% uncertainty for the sphere with which the HR1024i was calibrated was combined with the measurement uncertainty of multiple pre and post measurement sequence measurements made with the HR1024i of the sphere in the vertical orientation (**Figure 4B)**. A total of 12 measurements contributed to this uncertainty as in addition to the pre and post measurement sequence HR1024i measurements made with each of the three HSI instruments, three additional pairs of HR1024i measurements made when the equipment setup was rigorously assembled for other purposes. A relative measurement uncertainty of 0.15% to 0.33% is observed over most of the VNIR spectral range rising to 0.8% at the extremes providing a clear indication of the stability and repeatability of the measured sphere exit port measurements. Despite the lack of a complete uncertainty with the HR1024i calibration, this is significant in that it indicates that the uncertainty in the measurement process when the equipment configuration and data acquisition protocols carefully implemented, are dominated by the calibration of the calibration of the equipment, sphere, and HR1024i.

Absolute radiance data was acquired on Feb. 28th, Mar. 3rd and Mar. 12th, 2020 for the CASI, WISE, and µCASI instruments respectively. The absolute radiance produced following spectroradiometric calibration applied using standard processing techniques is compared to both the NRC sphere calibration results, following application of the orientation adjustment, and to the average HR1024i results. As is apparent in the relative difference results, all three of the instruments are better aligned with the HR1024i results than they are with the NRC calibration for wavelengths greater than approximately 450 nm. Considering only that wavelength range for now, the WISE results (**Figure 5A**) indicate a significant discrepancy over much of the spectral range that grows to as great as 20% (875 nm) with respect to the adjusted NRC calibration results and 12% (720 nm) with respect to the HR1024i results. Both the CASI (**Figure 5B**) and µCASI (**Figure 5C**) comparisons are, in general terms, better aligned than the WISE. The CASI relative difference varies from as little as -3% (525 nm) to great as -10% (> 850 nm) with respect to the NRC calibration and from 0% to -3% with respect to the HR1024i results. For the µCASI, the corresponding numbers are +2% (475 nm to 550 nm) to -9% (850nm) and +5% (560 nm) to -3% (680). This does not take into account the significant increase in the relative difference seen for wavelengths greater than 900 nm in the µCASI results which sees a rise to as much as 17% in the last channel. The µCASI data also exhibits a discontinuity in the relative difference results in the 550 nm to 575 nm region. A spectral leveling filter adhered to the surface of imaging detector chip is believed to transition at this wavelength. For wavelengths less than 500 nm, the relative differences for each instrument are similar regardless of the reference spectrum considered. For the WISE and CASI, the errors grow exponentially in the lower blue channels, starting at 430 nm and 500 nm respectively. The fall-off in accuracy for the CASI is much more significant, falling to -55% in its first channel (376.3 nm) whereas the WISE only falls off to -22% in channel 12 (coincidentally also 376.3 nm) and -43% in its first channel (361.5 nm). This is

consistent with the concerns previously raised with respect to the accuracy CASI radiance data at in its UV/blue wavelengths (Soffer et al. 2019). Despite the poor overall absolute calibration of the WISE, these two factors, the wavelength at which the roll-off starts in the absolute error and the magnitude of the absolute error in the UV/blue) are an indication of the expected enhanced blue performance of the WISE instrument with respect to the CASI. Despite the fact that the magnitude of the issue is not as significant and starts at a much lower wavelength in the WISE, these results suggest that the magnitude of the error is still significant enough to call into question any results below 400 nm.

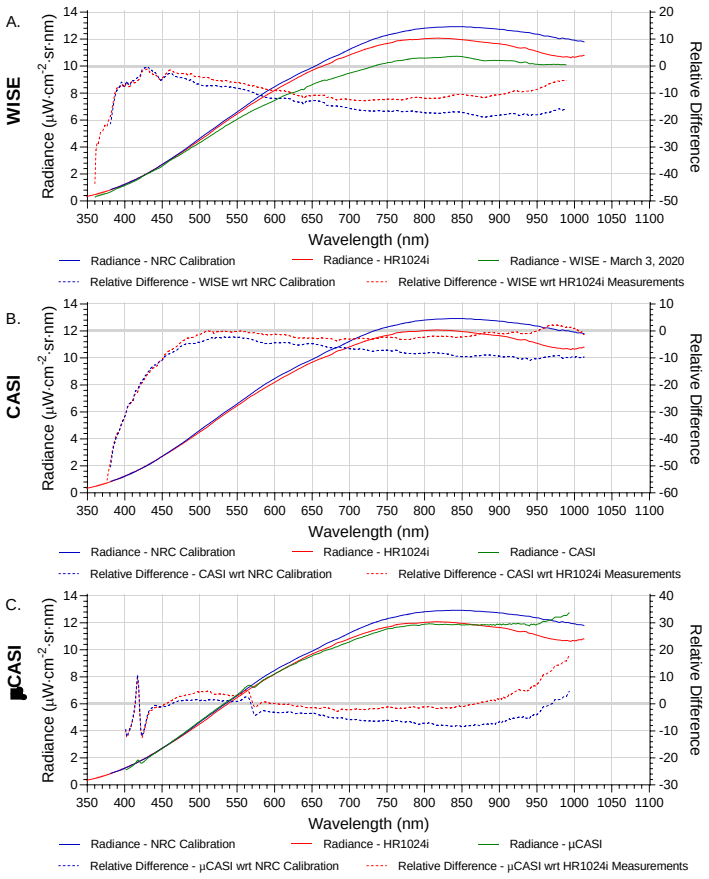

Figure 5. Absolute radiance of the sphere exit port radiance as derived from the spectroradiometrically calibrated (A) WISE, (B) CASI, (C) µCASI (solid green) in comparison with the vertically adjusted NRC calibration results (solid blue) and the HR1024i average results (red solid). The relative differences computed with respect to the NRC calibration (blue dotted) and the HR1024i (red dotted) are plotted on the secondary y-axis.

Even though the accuracy of the FPA-based µCASI below 435 nm is influenced by a significant spectral anomaly (±10%), there is no evidence of the blue end roll-off in absolute accuracy although it must be recognized that the instrument does not operate below 400 nm. The lack of roll-off in the blue absolute radiance accuracy in the µCASI results suggests that the issue is unlikely to be related to an error in the common calibration source used with all three

instruments. Rather it must be considered that the issue may be related to detector architecture and the accuracy of the applicable estimated offset corrections such as the FSS that influence the CCD frame transfer-based devices (WISE and CASI) and not the FPA-based µCASI. Likewise the increasing error noticed in the red end (> 900 nm) of the µCASI results may also be due to differences in the system architecture, specifically the manner in which the scattered light is estimated.

4.2 Secondary Comparison – Relative Radiance Validation

The 'stepped' imagery used to produce the cross-track measurement data set is shown for all three imaging spectrometers in **Figure 6**. It has been assumed that the integrating sphere output and the responsivity of the imaging spectrometer under test was stable over the period of data acquisition (WISE: IT = 48 ms/scan line x 541 scan lines ~ 26.0 s; CASI: IT = 48 ms/scan line x 435 scan lines ~ 21.9 s, µCASI: IT = 10 ms/scan line x 582 scan lines ~5.8 s). For the three channels used in the provided RGB images, the variability in the observed intensity levels are indications of imperfections in the uniformity correction. Variations in the observed colour suggest that imperfections that are spectrally dependent. In the calibrated WISE image, the 'strapping' structure used to bind together separate portions of the large CCD array resulting in decreased pixel sensitivities can be identified in three locations in the calibrated image (from the right hand side - start of the 3rd step, start of the 5th step, middle of the 9th step). In the CASI image, not only are their significant intensity and colour shifts apparent, but a significant step is visible between the right and left hand sides relating to the transition between the two CCD output ports and related readout electronics. For the µCASI, no intensity or spectral non-uniformities are apparent, possible being masked by the higher overall noise levels inherent within its data. Due to the extreme levels at which the imagery can be stretched, the magnitude of the non-uniformities generating these visual observations are challenging to interpret from these visual cues.

For each of the HSI instruments, the uniformity correction in the cross-track direction can be seen to be less than ideal when compared with the along-track results. For the WISE system (**Figure 7-A1**), the discrepancy appears most significant in the blue end (< 600 nm) whereas for the CASI it is more significant in the red end (> 600 nm). Assessment of the WISE results in terms of the generated absolute mean radiance levels produced using the two data extraction methodologies (along and cross-track) appear visually similar. When viewing the results in terms of the derived CoV, the cross-track results are significantly greater (worse) than those of the along-track results over then entire wavelength range. For the CASI (**Figure 7-B1**), a small but noticeable difference is observed in the absolute mean radiance levels, perhaps due to the intensity step between the right and left hands side pixels. The difference in the CoV between the cross-track and along-track results are more significant in the CASI results than those of the WISE between 600 nm and 980 nm and less significant for wavelengths < 600 nm. For the µCASI (**Figure 7-C1**), although the absolute mean radiance levels do not change significantly,

the degradation in the CoV due to the less than ideal uniformity correction with CoV results considerably larger than those produced by the WISE and CASI systems for wavelengths greater than 500 nm.

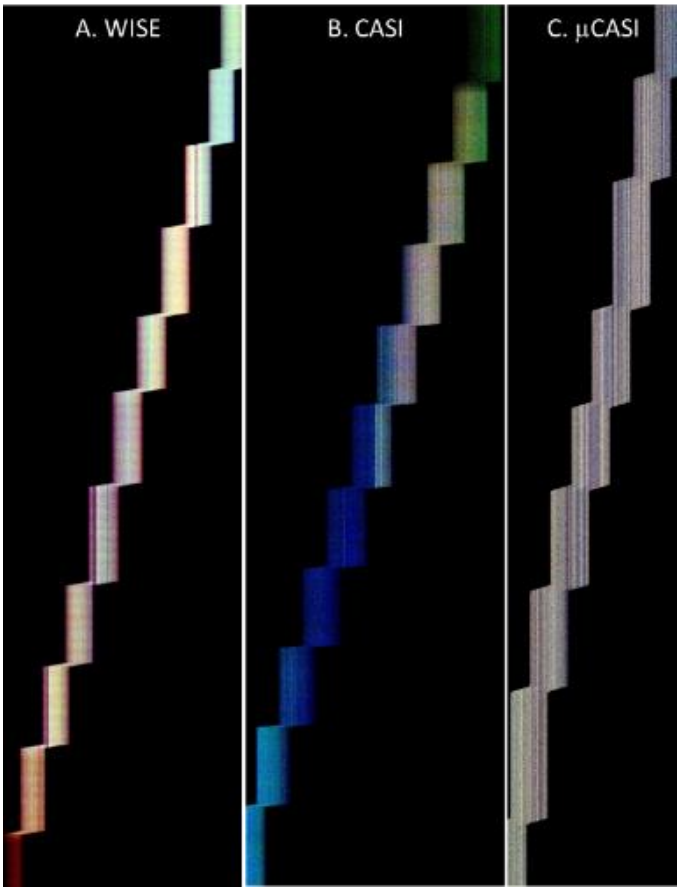

Figure 6. The stepped imagery (red ~ 650 nm, green ~ 550 nm, blue ~ 450 nm) acquired to generate the cross-track statistics are shown for the (A) WISE), (B) CASI, and (C) µCASI. The display look up tables for these images were established using a 2% linear enhancement of the centrally illuminated area.

For both the WISE and CASI the imperfections in the pixel-to-pixel corrections reduce the SNR level by more than a factor of 2 over much of the spectral range (WISE - **Figure 7-A2,** CASI (**Figure 7-B2**). The improvement in the µCASI SNR is much less significant (**Figure 7-C2**). Although the emphasise in the WISE design was to improve the system responsivity in the UV/blue channels as compared to the CASI, an improvement across the entire wavelength range was expected. This is consistent with what is being observed here. Blue channel improvements in the WISE over the CASI SNR derived from the along-track data set rise more than 900% at 375 nm (CASI ~ 2.2, WISE ~ 21.3), 230% at 400 nm (CASI ~ 12.5, WISE ~ 41) and 45% at 450 nm (CASI ~ 62, WISE ~ 90). For the channels near the SNR peak (~740 nm) the improvement remains near 45% (CASI ~ 255, WISE ~ 370). Corresponding SNR values for

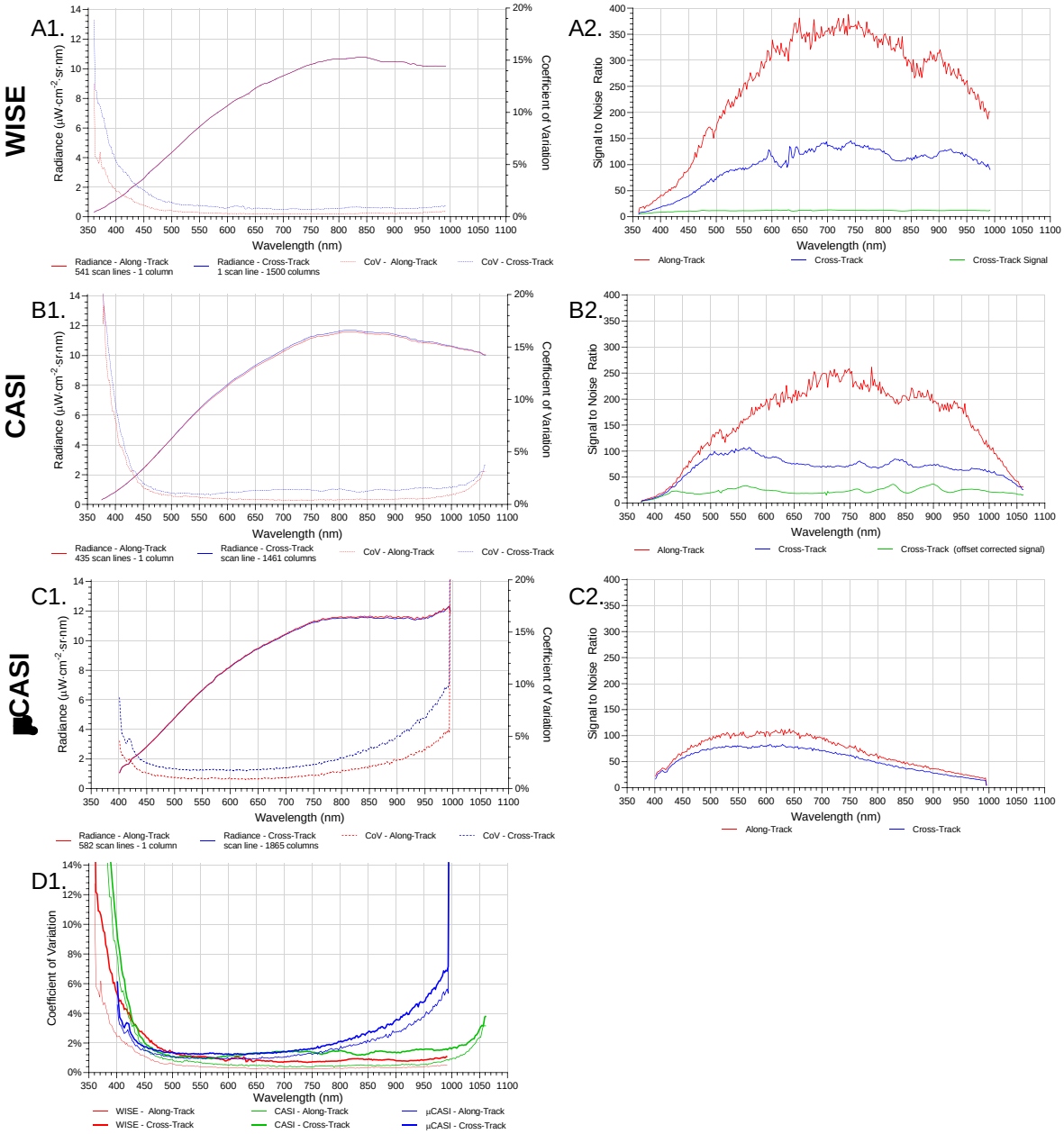

Figure 7. For the (A1) WISE, (B1) CASI, and (C1) µCASI, the absolute spectral radiance mean (solid lines) and CoV (dotted lines) generated for a single column (along-track) (red) and for the multipart ROI covering the entire FOV (cross-track) (blue) are provided. The CoV results for the three instruments are collected into a single chart (D1) to simplify visual comparisons of the results. Corresponding SNR results are provided in (A2) WISE, (B2) CASI, and (C2) µCASI. For the WISE and CASI instruments, the SNR cross-track data prior to spectroradiometric correction is also provide (green).

the µCASI are comparable to the WISE at 401 nm (21.8), comparable to the CASI at 450 nm (67) but does not compare in wavelengths greater than that peaking at ~ 100 and falling off much more significantly at wavelength > 700 nm. It is recognize that the sphere radiance levels that was approaching 12.0 µW/cm²/sr/nm for the wavelength at which the peak SNR was

observed, decreased to 0.73, 1.23, and 2.73 µW/cm²/sr/nm for the three reported wavelengths respectively. The implication here is that the decrease in the SNR spectrally is due to a combination of decreased sensitivity in the instruments themselves and the decrease in input radiance levels. It is also of note that the SNR of the WISE instrument prior to radiometric scaling (offset correct only) (green curve - **Figures 7A2**) is noticeable lower than that of the CASI (**Figure 7B2**) indicating that the range of pixel sensitivities in the WISE instrument is greater than that of the CASI.

4.3 System Linearity Assessment

The results generated from the HR1024i linearity data are used to validate the quality of the employed methodology. Although linearity of photodiodes are known to be extremely good, the photodetector employed in the integrating sphere has a broad spectral response (in this case with a photopic spectral response function). It is conceivable that the reported broadband response may not reflect changes that occur in narrower waveband regions. For example, a change that occurs at one spectral region may be compensated for by a corresponding change at another spectral location resulting in a spectral change that is not reflected in the broadband readout. As well, changes that occur outside or at the edges of the photopic response function of the photo diode will either not be reflected at all in the readout or contribute in a disproportionate manner. The HR1024i normalized linearity results (**Figure 8A)**, although significantly impacted by noise for data obtained below the 0.500% level, are seen to provide average spectral values approximating 1 for sphere readouts as low as 0.005%. Although it cannot be stated definitively that this indicates the radiometric output of the sphere exit port is linear as a function of the photodiode detector readout, it does indicate that the calibrated results derived from the recorded levels are. Since it is extremely unlikely that a non-linearity in the sphere output would be compensated for by a corresponding and opposite non-linearity in the HR1024i response resulting in a spectral normalized linearity of 1.0, the assumption is made that the sphere output radiance is indeed linear between 100.0% and 0.005% as reflected in the photodiode readout across the entire HR1024i VNIR wavelength region.

A number of similarities are apparent in linearity results produced from spectroradiometrically calibrated WISE (**Figure 8B**) and CASI (**Figure 9A**) data. For the WISE, the results appear linear to a sphere setting as low as 1.000% at which point nonlinearities (deviations from 1.0) begin to become apparent in the normalized linearity spectra, starting at the blue end, moving toward higher wavelengths with decreasing signal strength. For the CASI, a similar trend is apparent starting in the 5% data set. In addition, a similar response is observable at the upper wavelength end. Closer evaluation of the data identified that the non-linearity apparent at the spectral extremes is in fact an artifact of the manner in which the data was conditioned. The signal level at which the non-linearity becomes apparent is the level at which the noise inherent in the signal begins to rival the recorded signal levels following correction of the offset contributions. Since the output dataset following spectroradiometric calibration is recorded as an

unsigned integer, negative values generated at low signal level subject to negative noise levels of a larger amplitude will be truncated to a value of zero. Inclusion of such truncated values in the determination of the mean results in an artificial increase in the reported mean levels that in turn lead to the apparent non-linearity visible in the WISE and CASI normalized linearity plots.

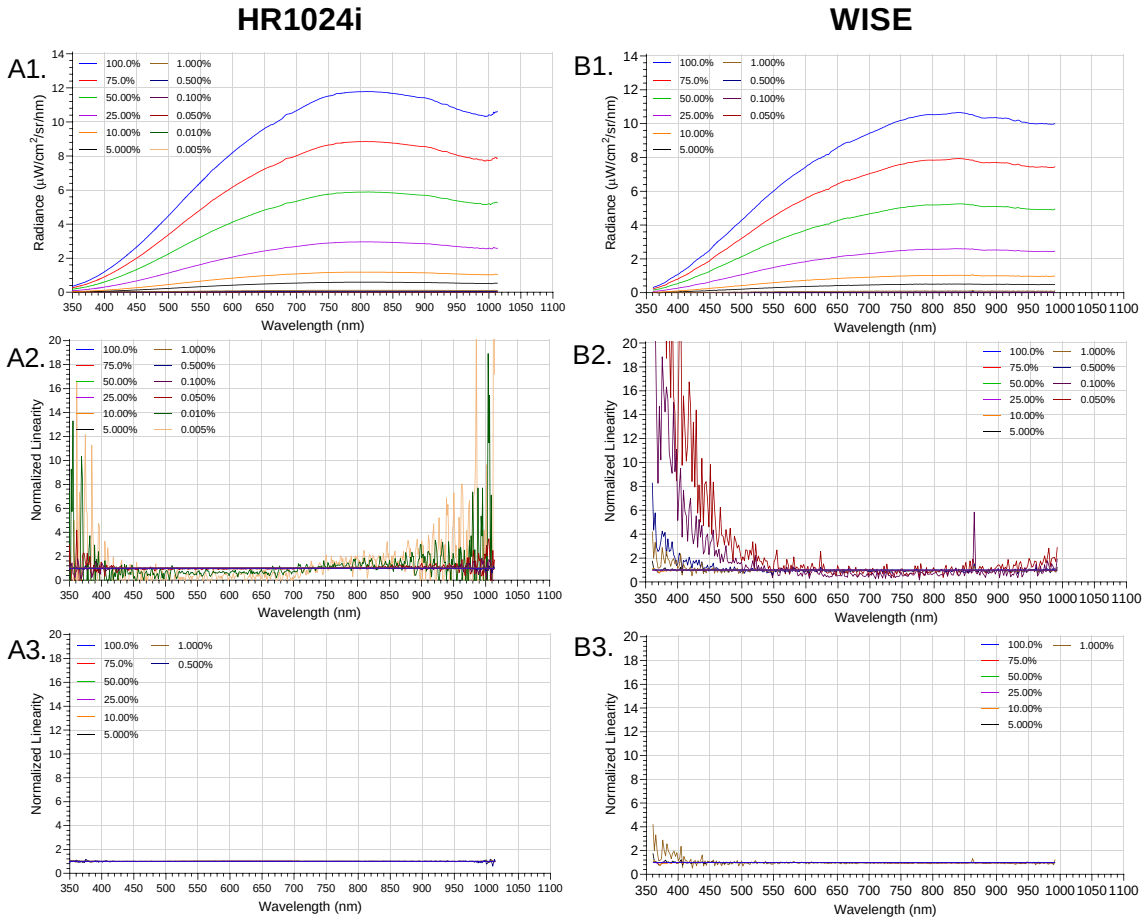

Figure 8. Non-Linearity assessment results for the (A) HR1024i portable spectroradiometer and (B) WISE HSI. Row 1) The radiance data following spectroradiometric calibration for each observed sphere setting. Row 2) The normalized linearity levels for all sphere measurement levels. Row 3) The normalized linearity levels with the lowest integrating sphere settings removed for clarity.

For the µCASI (**Figure 9B**), saturation is apparent in the 100.0% integrating sphere setting radiance results between 480 nm and 700 nm. The 75% measurement normalized by 1/0.75 was therefore used as the reference spectra for this data set. No evidence of a nonlinearity is apparent in the data with sphere setting as low as 0.05%. Noise levels significantly greater than the other instruments made measurements acquired at sphere levels less than 0.05% difficult to be interpreted. Further analysis of the data would have to be undertaken to understand why the µCASI is not impacted in a manner similar to the WISE and CASI by signal levels driven negative by noise contributions.

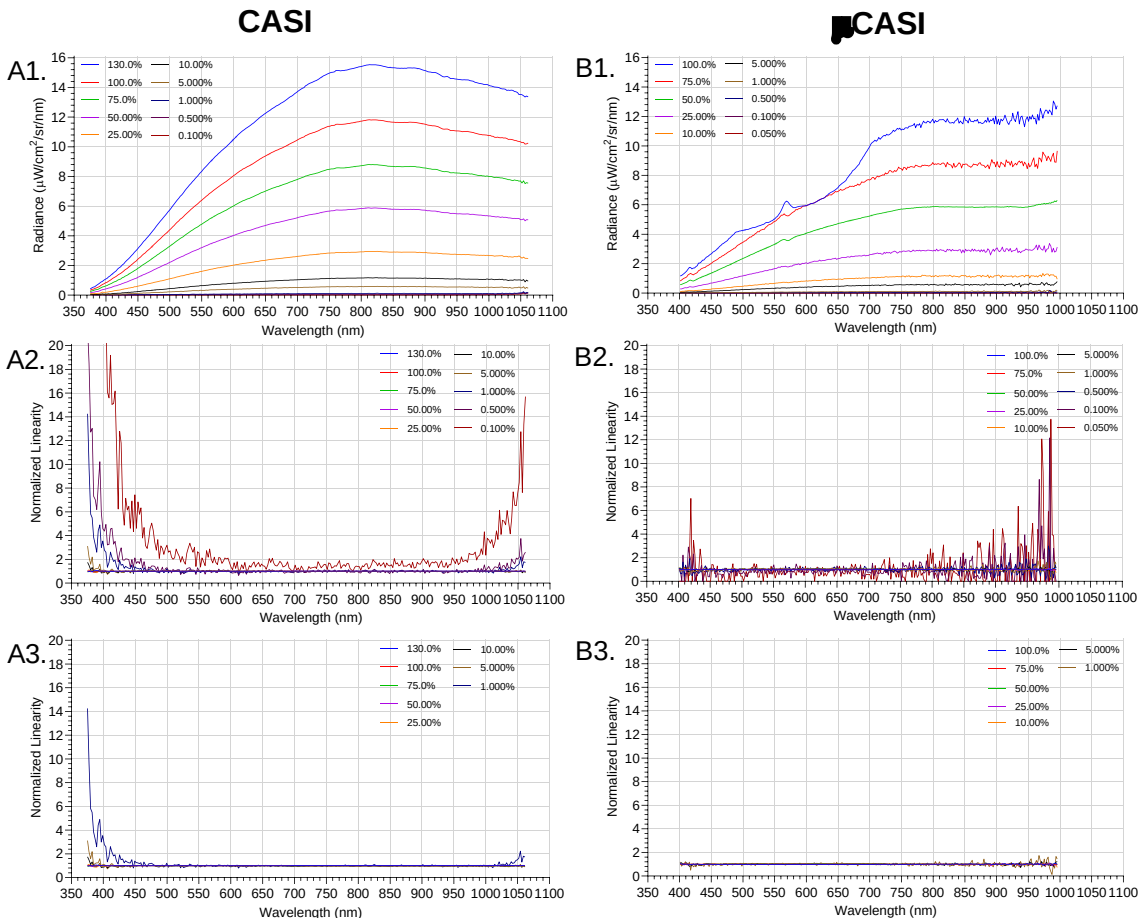

Figure 9. . Non-Linearity assessment results are provided for the (A) CASI and (B) µCASI HSIs. Row 1) The radiance data following spectroradiometric calibration for each observed sphere setting. Row 2) The normalized linearity levels for all integrating sphere measurement levels. Row 3) The normalized linearity levels with the lowest integrating sphere settings removed for clarity.

For each instrument, two 'calibration points' to be used in the application of a 2-point linear calibration refinement process avoiding the problematic low level input levels were selected (HR1024i - 100.0% and 5.00%; WISE - 100.0% and 25.0%; CASI - 100.0%; µCASI - 10.00%, and 75.0%). Radiance levels generated from the original spectroradiometric calibration (L_O) and following application of the 2-point calibration refinement (L_C) are provided in **Figure 10** for an example wavelength. The results are provided first in terms of radiance on the left hands side charts (column 1) then in terms of the residual errors on the right hands side charts (column 2). The residual errors are computed as the difference between the determined radiance values (L_O or L_C), and the expected radiance level defined as the 100.0% (75% for the µCASI) integrating sphere radiance scaled by the integrating sphere photodiode response for each of the measurements.

The quality of the original HR1024i calibration is apparent in the example data (λ = 402.8 nm) provided in the residual error levels provide in **Figure 10A**. Not only are the L_O residuals small but in addition there does not appear to be any improvements in the L_C residuals (peak residual

= 0.0025 µW/cm²/sr/nm for a nominal radiance level of 0.95 µW/cm²/sr/nm). What small residuals remain could potentially be the baseline non-linearity of the experimental setup. In the case of the WISE results (λ = 402.5 nm) (**Figure 10B**), a significant improvement is apparent in the L_C residuals over those of L_O with the peak residual dropping almost an order of magnitude from -0.12 to 0.017 µW/cm²/sr/nm. The refinement process has an even more significant impact on the CASI channel results (λ = 401.6 nm) (**Figure 10C**) with the L_C residuals dropping just over an order of magnitude from -0.485 to 0.046 µW/cm²/sr/nm following correction. It is important to realize that the peak L_O residual is dominated by issues related to low signal levels. Finally for the µCASI results (λ = 403.1) (**Figure 10D**), the residuals computed at 403.1 nm drop from -0.084 to 0.012 µW/cm²/sr/nm. Although issues remain in the low signal level results, the residual errors for the L_C data points with healthy signal levels ($L_O > \sigma_{LO}$) approach zero.

The discussion in the previous paragraph only assesses a single channel. A complete appreciation must evaluate what is occurring across all channels (512 for the HR1024i, 288 for the three HSI instruments). This can best be achieved by looking at the spectral gain and offset derived from the 2-point calibration refinement process (**Figure 11** – column 1) with the gain plotted on the primary y-axis and the offset plotted on the secondary y-axis. Following application of the gains and offsets on a channel by channel basis, the impact of the correction process can be observed in a comparison of the spectral plots of the root mean squared (RMS) residuals of L_C against that of L_O (**Figure 11** - column 2).

Gains and offset generated for the HR1024i (**Figure 11A1**) approximate values of 1.0 and 0.0 respectively, those expected for a perfect calibration, across the entire spectral range. Subsequently the spectral RMS residual errors (**Figure 11A2**), do not indicated any improvement by the application of these parameters in the refinement process as is apparent in a comparison of the max and mean spectral RMS residual provided in **Table 1** for the original (L_O) and corrected (L_C) data.

In comparison, the WISE spectral gains and offsets (**Figure 11B1**) deviate substantially from their ideal values. The gain rises sharply for wavelengths below 425 nm to as large as 1.702 in the first channel. For wavelengths greater than 460 nm, a concave down shape is apparent peaking at 1.134 at 684 nm. For wavelengths less than 650 nm, the offsets parameter maintains a value near 0.0 µW/cm²/sr/nm (-0.01 to +0.03 µW/cm²/sr/nm) indicating that the system response provided in the original spectroradiometric calibration is linear as it trends through the origin (0-0 point) based upon the two data points (IS settings 100.0% and 25.00%) used to generate the refinement parameters. The offset however rises between 600 nm and 725 nm then maintains a value of between +0.07 and +0.10 µW/cm²/sr/nm indicating that there is an offset contribution that is not being properly adjusted for in the original calibration process. The location of this rise, at roughly twice the wavelength of the first channel, and the fact that the offset remains relatively constant at wavelengths beyond that, is suggestive of a second order diffracted light issue. The impact of the radiance refinement is apparent in the large difference in

the RMS residual error (**Figure 11B2**). The significance of the improvement are evident in the improvement in the WISE maximum/average spectral RMS residual values provided in **Table 1**.

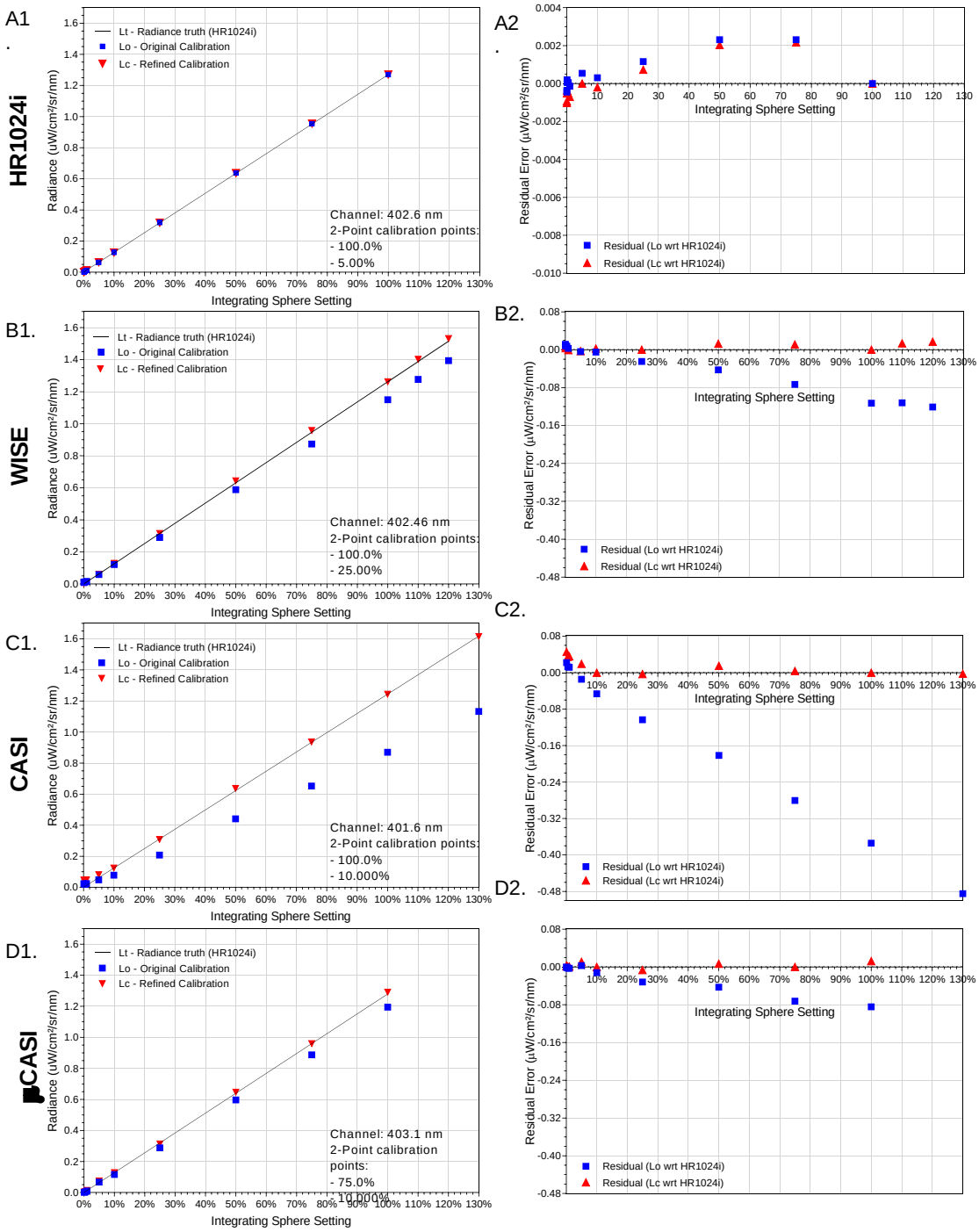

Figure 10. Non-Linearity assessment results for an example wavelength of approximately 402 nm with respect to the 100.0% measurements (75% scaled to 100% for the µCASI) for the (A) HR1024i, (B) WISE, (C) CASI and (D) µCASI instruments. The right hand charts (column 1) show the radiance value generated from the original spectroradiometric calibration (L_O) (■) and following a two point calibration refinement (L_C) (▼) compared with that of a perfect linear results (black). The left hand charts (column 2) show the corresponding residual errors for the (L_O) (■) and (L_C) (▲) data.

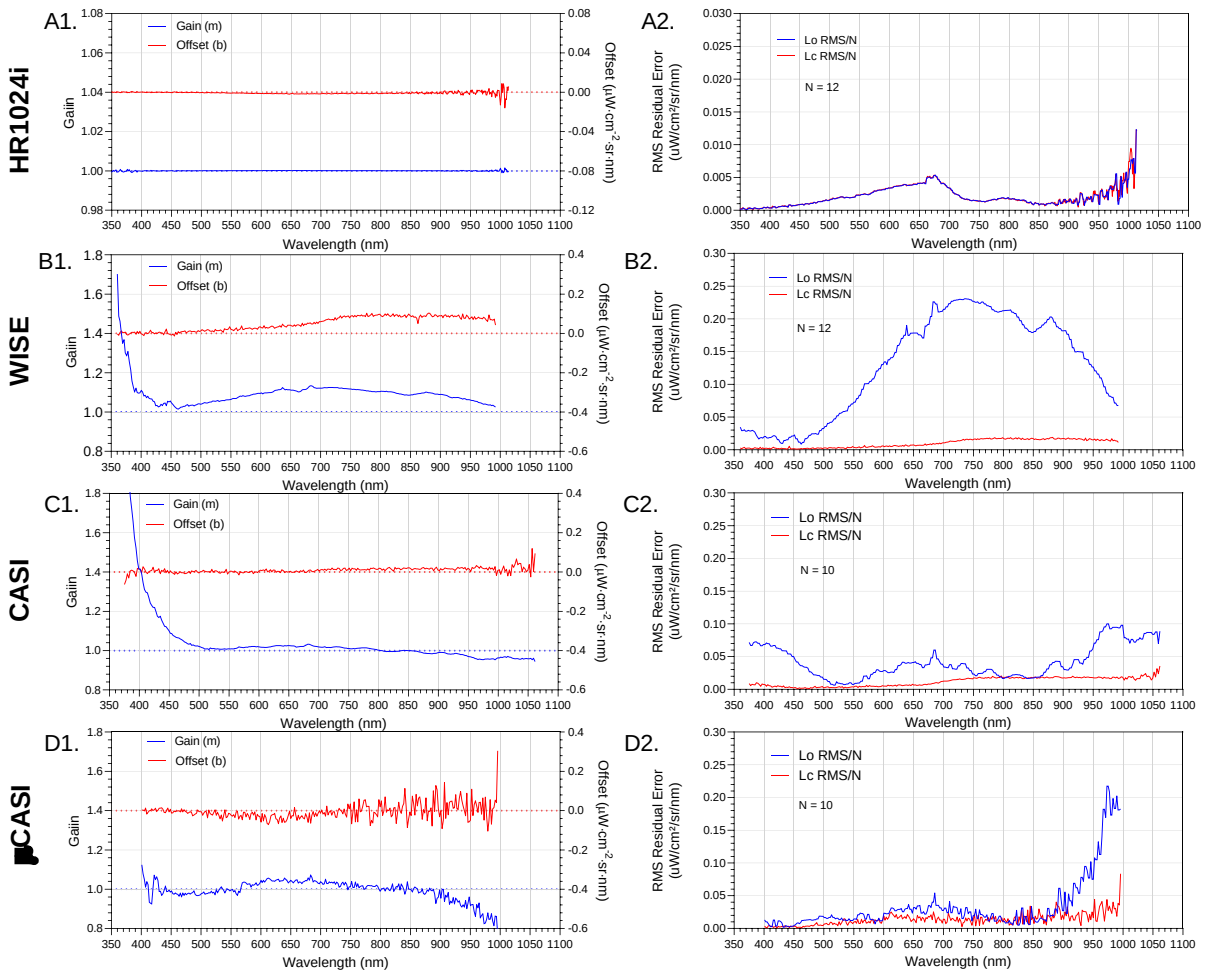

Figure 11. Spectral gains (blue) and offsets (red) as computed within the 2 point calibration refinement process, as defined in **Figure 10,** are provided for the HR1024i (A1), WISE (A2), CASI (A3), and µCASI (A4). The RMS residual error of the originally calibrated radiance data (Lo) (blue) and following calibration refinement (Lc) (blue), defined as the average RMS error with respect to the HR1024i measurement of the integrating sphere set to 100.0%, are provided for the HR1024i (A2), WISE (B2), CASI (C2), and µCASI (D2). Note the different scales used in the HR1024i (A1, A2) charts.

Table 1: RMS residual statistics extracted from spectral data as shown in **Figure 11** column 2.

	HR1024i	WISE	CASI	µCASI
RMS Residual Max (L_O) (µW/cm²/sr/nm)	0.00535	0.2307	0.1000	0.2173
RMS Residual Mean (L_O) (µW/cm²/sr/nm)	0.00213	0.1293	0.0417	0.0340
RMS Residual Max (L_C) (µW/cm²/sr/nm)	0.00536	0,01905	0.0356	0.0835
RMS Residual Mean (L_C) (µW/cm²/sr/nm)	0.00215	0.0096	0.0118	0.0139

The CASI gain (**Figure 11C1**) deviates only slightly from unity (±0.025) within the central portion of the spectrum (500 nm to 940 nm). The gain at the red end (> 940 nm) drops but only slightly to 0.995. At the blue end of the spectrum the gain deviates exponentially to as great as 2.4 in the first channel (375.3 nm) consistent with the problems previously noted in the blue end. This is significant greater than the 1.3 reported for the WISE channel at the nearest channel (375.9 nm), once again reflecting the WISE's improved sensitivity in the blue channels. Whereas the offset is relatively small (0.0 -0.022/+0.032 µW/cm²/sr/nm) between 395 nm and 1000 nm, the extreme channels appear to be influenced by increasing noise levels with a slight drop-off apparent at the blue end. While the improvement introduced by the refinement process is nowhere near as substantial as with the WISE, significant improvements are still realised in the blue and to a lesser extend the red end. The residual RMS results (**Figure 11C2**) indicate there are two spectral regions (525 nm to 560 nm and 780 nm to 865 nm) in which the calibration refinement does little to improve the accuracies. The overall improvement is once again evident in maximum/mean RMS residual parameters provided for the CASI instrument in **Table 1**. The spectral RMS residual is noted to have a similar shape to that of the WISE (a rise in the residuals between 675 nm and 725 nm) despite the fact that a similar feature is not apparent in the CASI offsets.

The most apparent item of note in the µCASI spectral gains/offsets and RMS (**Figure 11D1)** residuals is the substantially higher noise levels. Although more significant noise is noticeable over the entire spectral range, there is a significant increase above 750 nm. Despite this, the gains and offsets are observed to track nicely within the noise envelopes with the ideal values of 1.0 and 0.0 µW/cm²/sr/nm. The exception to this is a spectral feature located just below 450 and a drop off above 900 nm apparent in the gain values. Improvements in the RMS residuals spectra (**Figure 11D2**) are small in comparison to those witnessed in the WISE and CASI systems. The exception to this is once again the spectral region above 900 nm. The apparent improvement seen in the maximum/mean provided for the µCASI in **Table 1** is driven by the improvements achieved in that portion of the spectrum.

5 Conclusions

A methodology has been developed, implemented, and, to a preliminary level, validated using equipment currently available at FRL to assess the quality of the FRL operated VNIR HSIs in terms of 1) absolute spectroradiometric accuracy, 2) relative accuracy (uniformity correction), and 3) system linearity following spectroradiometric calibration. The principal equipment essential to the implementation and validation of this methodology were the Hoffman LS-65-8C Luminance Standard (6”) Sphere, the SVC HR1024i portable spectroradiometer, the computer controlled Newmark XY translation stages, and a platform capable of mounting the HSI equipment in a nadir viewing orientation.

As previous investigations of airborne CASI data had suggested, significant absolute spectroradiometric calibration errors were identified in the UV/blue portion of the VNIR spectral range within not only the CASI (< 500 nm), but also the WISE (< 425 nm) with errors in channel 1 as large as 55% (376.3 nm) and 45% (361.5 nm) for the two instruments. In addition, the WISE system has a spectrally variable error in the absolute calibration results over the remainder of the VNIR spectral region with errors between 0% and -12%. This compares with an absolute calibration error of 0 to -3% for the CASI. For the µCASI, the blue end radiometric problem is not apparent suggesting that the origin of the absolute calibration error is not due to an error inherent in the calibration source used by all three sensor systems. With the exception of a couple of narrow spectral features (400 nm to 435 nm and 560 nm to 580 nm) and a rising error in the red end (> 900 nm), the absolute accuracy of the µCASI is good (± 2%). With the relatively good radiometric calibration accuracy of the CASI and µCASI, it is believed that the error in the WISE results is due to a shift in the system response that has occurred since its calibration.

The assessment of the uniformity correction show significant issues remain in the process for both the WISE and CASI systems. These issue results in the reduction of peak SNR levels from 370 to 150 in the WISE and 250 to 100 in the CASI. Although the SNR levels are much lower for the µCASI, the impact of the deficiencies in the uniformity correction are much less significant with peak SNR levels dropping from 100 to 80. Since these results were generated from a single intensity measurement, it is unclear if the relatively impact would be the same at other input levels.

Concerns with the initial assessment of the WISE and CASI linearity were subsequently discovered to be due to the manner the data was conditioned having an impact on extremely low signal level data encountered in the UV/blue portion of the spectrum. Ultimately it was concluded that no issues were identified in the linearity of any of the HSI instruments. With the linearity of the systems confirmed, the utility of using a linear 2-point calibration refinement similar to that commonly applied to the refinement of airborne hyperspectral imagery was assessed. The mean RMS residual error of the linearity assessment data sets are shown to

significantly improve following application of the refinement process. Due to the large absolute calibration error in the WISE results, the impact is significant, reducing the mean RMS residual error to 0.0096 µW/cm²/sr/nm from 0.1293 µW/cm²/sr/nm. For the CASI the impact, although far less significant, remained substantial over large portions of the VNIR spectrum reducing the mean RMS residual error to 0.0118 µW/cm²/sr/nm from 0.0417 µW/cm²/sr/nm. The impact on the µCASI was almost non-existent with the exception of wavelengths greater than 800 nm, reducing the mean RMS residual error to 0.0139 µW/cm²/sr/nm from 0.0340 µW/cm²/sr/nm.

The results generated by this methodology have consistently identified the improvement in the WISE system response as compared to the CASI within not only the UV/blue spectral range but over the entire VNIR spectrum.

Validation of the methodology came in the form of application of the processes to data acquired with the HR1024i portable spectroradiometer. The HR1024i did not provide the same integrating sphere exit port radiance levels as provided by the NRC calibration. However, the decision was made to use the radiance spectrum generated by the HR1024i as the reference as the data of the sphere had been acquired in the same configuration, environment, and time as the HSI data against which it was compared. Although the comparison numbers identified in this report will be influenced by this decision, the conclusions in general will not be impacted. Repeated measurements of the sphere exit port radiance with the HR1024i have quantified the stability/repeatability of the measured output as much less significant that the uncertainties associated with equipment. In addition, the HR1024i was able to confirm the linearity of the sphere exit port radiance as a function of the reported photo-diode readout.

Repeated implementation of the described methodology with the FRL HSI instrumentation, when combined with a spectral stability check, is capable of providing a rigorous assessment of the system health and stability. Such efforts will provide critical insights into the quality of the data products being generated for FRL clients as well as providing a critical assessment of when the systems need to be sent out for new calibrations. Although the methodology has not been applied at this time to the SWIR HSI sensor operated by FRL, no reasons have been encountered that would suggest it would not be applicable.

6 References

Arroyo-Mora, J.P., Kalacska, M., Inamdar, D., Soffer, R., Lucanus, O., Gorman, J., Naprstek, T., Schaaf, E.S., Ifimov, G., Elmer, K., & Leblanc, G. (2019). Implementation of a UAV–Hyperspectral Pushbroom Imager for Ecological Monitoring. *Drones, 3*, 12

Arroyo-Mora, J.P., Kalacska, M., Soffer, R., Ifimov, G., Leblanc, G., Schaaf, E.S., & Lucanus, O. (2018). Evaluation of phenospectral dynamics with Sentinel-2A using a bottom-up approach in a northern ombrotrophic peatland. *Remote Sensing of Environment, 216*, 544-560

Arroyo-Mora, J.P., Kalacska, M., Løke T., Schläpfer, D., Coops, N.C., Lucanus, O., Leblanc, G. (Under Review) Assessing the impact of illumination on UAV hyperspectral imagery collected under various cloud cover conditions. 2020. Remote Sensing of Environment.

D'Amato, D. (1998). *Spectral radiance and temporal stability of a uniform radiance source integrating sphere with enhanced blue performance*. SPIE

Ilori, C.O., Pahlevan, N., & Knudby, A. (2019). Analyzing Performances of Different Atmospheric Correction Techniques for Landsat 8: Application for Coastal Remote Sensing. *Remote Sensing, 11*, 469

IOCCG (2000). Remote Sensing of Ocean Colour in Coastal, and Other Optically-Complex Waters. In S. Sathyendrath (Ed.), *Reports of the International Ocean-Colour Coordinating Group*. Dartmouth, Canada: IOCCG

ITRES Research Ltd. (2010). CASI-1500 Calibration Manual. In. Calgary, AB, Canada: ITRES Research Limited

ITRES Research Ltd. (2017). RCX Manual. In. Calgary, AB, Canada: ITRES Research Limited

Janesick, J.R. (2001). *Scientific Charge-Coupled Devices*. Bellingham, Washington: SPIE—The International Society for Optical Engineering

Kalacska, M., Arroyo-Mora, J.P., Soffer, R., & Leblanc, G. (2016). Quality Control Assessment of the Mission Airborne Carbon 13 (MAC-13) Hyperspectral Imagery from Costa Rica. *Canadian Journal of Remote Sensing, 42*, 85-105

Ogashawara, I., Mishra, D.R., & Gitelson, A.A. (2017). Chapter 1 - Remote Sensing of Inland Waters: Background and Current State-of-the-Art. In D.R. Mishra, I. Ogashawara, & A.A. Gitelson (Eds.), *Bio-optical Modeling and Remote Sensing of Inland Waters* (pp. 1-24): Elsevier

Qian, S., Bergeron, M., Djazovski, O., Maszkiewicz, M., Girard, R., Kappus, M., Bowles, J., Mannino, A., Matuszeski, A., Furlong, M., Ardouin, J., Fournier, G., Levesque, J., Moreau, L., Lavigne, J., Mandar, J., Busler, J., & Buttner, G. (2017). A spaceborne coastal and inland water color hyperspectral imager. In, *2017 IEEE International Geoscience and Remote Sensing Symposium (IGARSS)* (pp. 447-450)

Qian, S.E. (2020). *Hyperspectral Satellites and System Design*. CRC Press

Richter, R., & Schläpfer, D. (2019). ATCOR-4 User Guide, Version 7.3.0. In (p. 196): ReSe Applications LLC

Slater, P.N. (1980). *Remote Sensing, Optics and Optical Systems*. Addison-Wesley Publishing Company

Soffer, R.J., Ifimov, G., Arroyo-Mora, J.P., & Kalacska, M. (2019). Validation of Airborne Hyperspectral Imagery from Laboratory Panel Characterization to Image Quality Assessment: Implications for an Arctic Peatland Surrogate Simulation Site. *Canadian Journal of Remote Sensing, 45*, 476-508

SVC (2019). Field Spectroscopy Guide with SVC i-series Spectroradiometers. In: Spectra Vista Corporation

Appendix A: HR1024i Operational Considerations

The HR1024i portable spectroradiometer is designed primarily for use as a field spectrometer. Use of this instrument in the field along with the operational issues that are inherent in that environment results in absolute accuracies that are significantly less than that required to perform the lab assessment being reported here. Previous use of the instrument in the lab to perform panel characterization measurements have identified a number of issue that must be carefully considered to acquire and assess the data acquired here. It must be noted that all previous use of the instrument at FRL, both in the field and in the laboratory, made use of relative measurements in which the stability of the instrument response between the comparative measurements was of primary concern. In many of the measurements performed within this work described here, absolute measurements are being evaluated. In this case, the stability between the system response at the time of the acquisition of the absolute calibration data set and the time of the test data is of concern.

In this appendix, a number of issues are identified and addressed below in terms of their potential implications on the data set acquisition and assessment.

- **Ensure that the HR1024i was provided adequate time to thermally stabilize.** When viewing HR1024i results in absolute radiance terms, this issue must be considered in a more restrictive manner than simply allowing adequate time to stabilize. The reported temperature of the VNIR detector, which is not temperature controlled, during the data collection is best acquired at an identical temperature to that at which the calibration data was acquired in order to provide the most accurate results. As the temperature varied from the calibration set point, spectrally dependent variations occur that are not only noticeable across the VNIR detector channels but also within the extreme spectral channels of the SWIR1 detector. The impact on the SWIR1 detector data is interesting as unlike the VNIR detector, it is temperature controlled to a constant temperature. Evaluation of the reported detector temperature over numerous data sets, acquired both in the lab and in the field, are -4.7 ± 0.1°C for the SWIR1 detector (-9.8 ± 0.1°C for the SWIR2 detector). It has been suggested that the impact on the SWIR1 results could be a secondary effect related to the fact that the reported VNIR detector temperature reflects the ambient temperature within the instrument and therefore may impact the readout electronics resulting in minor changes to the conversion sensitivities. With the low sensitivity and subsequent low raw signal levels encountered, the extreme SWIR1 channels would be particularly sensitive to such variations. Although not specified within their calibration report, SVC reported that that the VNIR temperature of the data sets used to produce the calibration data was 36.6° C. SVC does provide a proprietary algorithm to correct for discontinuities between the overlapping VNIR/SWIR1 channels that are found for our instrument in the 370 to 1013 nm range. This effectively is supposed to correct for temperature sensitivities by making use of the temperature

stability and supposed signal stability found within SWIR1 channels. Our evaluations show that the results, produced by the application of this process, are inadequate for the accuracy/precision requirements of the work being performed here. Note that tying the VNIR temperature to that of the absolute calibration measurements was not an issue when using relative HR1024i measurements as is normally done during the field reflectance measurements or panel characterization measurements performed in the lab. In those cases, the issue of importance is that both the reference and target scans be acquired at similar temperatures (< ± 0.2), which is something that is confirmed for within the standard processing approach.

- **Ensure that the HR1024i FOV was completely within the integrating sphere exit port.** The FOV of the fore-optics in use is nominal 4. Ensuring that the instrument FOV is completely within the sphere exit port is of particular concern since observations of the exit port were performed in the near-field and its impact on the sharpness of focus is unknown. The computed diameter of the nominal 4° FOV at the nominal lens-to-port vertical (Z) separation distance of 17.0 cm is 1.2 cm. This is significantly smaller than the 4.0 cm diameter of the exit port hopefully allowing for the less than ideal focus encountered at this separation distance. With these concerns in mind a pair of tests were performed to confirm that the measured response did not vary as a function of the separation distance nor due to minor changes in the XY (horizontal position). First, one time measurements were performed with HR1024i vertical separation varied between 10 cm (FOV 0.7 cm) and 43 cm (FOV = 3.1 cm). Each measurement was ratio'd against the 10 cm measurement. Noticeable changes in the spectral ratio were not apparent as a function of separation distance even at 43 cm implying that (1) the FOV, even at the greatest separation distance, was located wholly within the exit port uninfluenced by edge-effects; and (2) the radiometric uniformity of the exit port did not introduce observable variabilities as the FOV within the exit port increased with distance.
- **Assessment of physical configuration for optical coupling effects.** Optical coupling is a phenomena in which inter-reflectance occur between two surfaces facing each other. In this case those inter-reflectance would result in additional radiance being returned into the integrating sphere thereby impacting the apparent output radiance of the sphere. This phenomena is readily apparent in the increases observed in the sphere monitoring photodiode readings if one places their palm opposite the exit port and slowly decreases the separation. As this effect will be a function of the square of the separation distance, then if the separation test described above should also provide an indication of the level of optical coupling experienced in this configuration. As indicated above, observable changes were not observable in the relative radiance measurements nor were they apparent in the sphere monitoring photo diode readings as the separation increased.
- **Centering of HR1024i within and radiometric uniformity of sphere exit port.** Following a preliminary effort to visually align the HR1024i FOV with the centre of the exit port at the nominal separation distance of 17 cm, the XY translation stage was used

to translate the sphere beneath the HR1024i. The location at which the HR1024i measurement began to be impacted by edge effects on either side of the centre position was noted as the 'edge' position. The centre position was then adjusted to the midpoint between the two positions. This was repeated iteratively for both the X and Y axis to arrive at a final centre alignment. Once the location was identified it could be accurately re-established throughout the period of a measurement sequence using the XY translation stages. An examination of the horizontal (x and y -axis) relative radiance profiles (xy position measurement divided by the centre point measurement) with those impacted by edge effects excluded, did not exhibit any non-uniformity's that rose above the residual noise levels. Despite this apparent independence of the absolute radiance levels with respect to observed position within the exit port efforts were made during the commissioning of each instrument configuration to centre the HR1024i FOV within the exit-port and to carefully re-centre it before each measurement.

- **Ensure that the integrating sphere exit port radiance remain unchanged with respect to that observed during the NRC calibration.** Once established, the integrating sphere monitoring photodiode at any setting was found to remain stable to within the most significant readout digit (0.1% for 60.0% to 132.0%, 0.01% for 20.00% to 60.00% and 0.001% from 0.005% to 20.00%). In addition, each time the sphere was set to 100.0% in order to perform an absolute calibration measurement, the Vernier aperture setting was recorded. For all recorded measurements made in the vertical orientation with the Integrating sphere located below the HSI instrument under test and the HR1024i, the Vernier position was identical at .803" ± 0.001" (TBC). Not only is this an indication that the radiometric output of the sphere remains stable but that the setup can reliable be recreated without impact to the observed radiance levels. In addition the integrating sphere stabilized power supply voltage level which was found to remain unchanged (15.752 ± .001 V) during all measurement sequences and in fact has remain unchanged since its original 1993 calibration. It can be inferred from this later observation that it is unlikely that a colour change in the bulb or sphere wall reflectance (yellowing) would have occurred while retaining the same photodiode output. It is not known what the Vernier setting was at the time of the 1993 calibration so a similar statement cannot be made with respect to changes since the original calibration.
- **Long-term stability of the HR1024i.** The long-term stability of the HR1024i was further assessed by comparison (wavelength and radiometric sensitivity) of the 2018 calibration results with the current 2020 calibration. The minimal shifts in the channel wavelength registration (0.0 to +0.3 nm) and variances of between -2.5% and 4.2% in the radiometric sensitivity response for the VNIR portion of the detector suggest remarkable long term stability for an instrument that has seen significant use both in the lab and field environments. The changes to the radiometric sensitivities in fact look similar to the relative spectral shape witnessed when temperature fluctuations of the reported VNIR detector temperatures of an otherwise stable source is encountered. It is thus conceivable that the small changes could be further explained due to the differences in

the VNIR detector temperatures that was reported as 35.2°C during the 2018 calibration as compared to 36.6°C for the 200 calibration. Further assessment which would require the development and verification of a temperature compensation would have to be performed to confirm this as the manufacturer supplied methodology does not provide the required accuracies.

- **Integration time instabilities.** The HR1024i can be configured to either automatically set the integration time or to have it manual set. The automatic setting option is commonly used in order to assure that the integration time applied is optimal for the target radiance levels encountered. An unexplained scenario has been found to arise in which the integration time settings will change in automatic mode despite the fact that the observed radiance levels remain unchanged (i.e., change from 100 ms to 70 ms while watching the stable integrating sphere). In such a circumstance, relative measurements, which should results in a spectral ratio of 1, have been noted to have multiple spectral anomalous across the VNIR spectral region. It is of considerable interest therefore that these or similar anomalies are not apparent in the linearity results derived with the HR1024i and reported on in this report.

Appendix B: Hoffman Luminance Standard Sphere Spec Sheet

1 *Offered at* Best Price

HOFFMAN LUMINANCE STANDARD SPHERE

Integrating Sphere

... other images

Location: Scotia, New York

Unit Price	Unstated
Number of Units	1
Manufacturer	Hoffman
Model	LS-65-8C
Diameter	6.000 in (15.2 cm)
Output Ports	2
Light Source	Halogen
Accessories	Controller/Power Supply Model LS-65-8C HO
Other Information	Luminance: Luminance range at 2856 Kelvins of 0 to 350 foot lamberts High stablitiy qaurtz halogen lamp: 30 W on low output units, 80 W on high output units Uniformity: • ±0.05% typical over 25mm diameter • ±0.1% typical over 40mm diameter Accuracy: ±2% Stability: ±0.2% or 0.02 Ft-L for 8 hours at 23°C Calibrated color temperature range of 1800 to 3000 Kelvin Sphere assembly dimensions: 7"W x 9.5"D x 12"H; 6 lbs.
Power Requirements	115/ 230 V 3.0 A 50/60 Hz 1 Phase
Weight	15 lb (7 kg)

Appendix C: NRC Spectral Radiance Calibration – Hoffman Engineering Spectral Radiance Standard

National Research Council Canada
1200 Montreal Road
Ottawa, ON K1A 0R6

Conseil national de recherches Canada
1200, chemin de Montréal
Ottawa (Ontario) K1A 0R6

NRC·CNRC

NRC Calibration Report Number: PAR-2020-3684 Date of Issue: 2020-02-25

CALIBRATION REPORT

Spectral Radiance Calibration
Hoffman Engineering Spectral Radiance Standard
Model RS-658CH0, s/n 485

for

NRC Flight Research Laboratory-Aerospace
Building U-61
Ottawa, Ontario
Canada K1A 0R6

Attention: Raymond Soffer

Client order number: internal NRC order number: internal

Metrologist:

Dr. Amin Rasoulof, Research Officer
Amin.Rasoulof@nrc-cnrc.gc.ca
(613) 991-2399

Authorized by:

Dr. A.A. Gaertner, Project Leader
Arnold.Gaertner@nrc-cnrc.gc.ca
(613) 993-9344

Results in this report are traceable to the International System of Units (SI) through national measurement standards maintained at the National Research Council of Canada.

Results in this report relate only to the items being calibrated. Issuing of this report does not constitute an approval of the customer's products or procedures by the NRC.

Les résultats dans ce rapport sont traçables au Système international d'unités (SI) par l'intermédiaire des étalons nationaux de mesure maintenus au Conseil national de recherches du Canada.

Les résultats contenus dans ce rapport ne se rapportent qu'aux objets étalonnés. L'émission de ce rapport ne signifie pas l'approbation des produits ou procédures du client par le CNRC.

Canada

1.0 Introduction

A Hoffman Engineering Spectral Radiance Standard Model RS-658CH0, s/n 485, with power supply, was received at NRC-M36 on 2020-January-27. The equipment was hand carried by Raymond Soffer of NRC Aerospace Flight Research Laboratory, Ottawa, Ontario.

The calibration requested was the spectral radiance (380 nm to 1068 nm at 4 nm intervals) at the centre of the sphere port for an aperture setting (micrometer) that resulted in a reading of 100% on the power supply display for the "Radiance Level / 100%" dial setting of the power supply. It was also requested that the micrometer setting and the "Radiance Level / Lamp Voltage" values be reported, and that the spectral radiance be measured for a spot size diameter approximately one-half the diameter of the Hoffman RS658CH0 sphere output port.

The measurements and calibrations were carried out on 2020-February-04/05/06.

The equipment was picked up by Raymond Soffer of NRC Aerospace on 2020-February-24.

2.0 Calibration Procedure

The spectral radiance measurements and calibrations were performed using a Photo-Research Model PR-715 Spectroradiometer (s/n 75012201). The PR-715 was calibrated using the known spectral radiance of a pressed polytetrafluoroethylene (PTFE) diffuser illuminated by calibrated spectral irradiance source standards. The geometry used was 0°/45° (incidence/reflection). Two National Research Council spectral irradiance standards were used (FEL #91498 and #91499), each at three distances from the PTFE diffuser, to produce six different spectral radiance levels and corresponding PR-715 measurements. Each PR-715 measurement was an average of three measurement integration cycles. The calibration of the PR-715 was performed on 2019-October-31 using PAR QMS procedure PAR-126v0.0.

The spectral radiance at the Hoffman RS658CH0 sphere output port, normal to the plane of the output port, and centered on the output port, was measured using the PR-715. The measurement aperture of the PR-715 was set to 1 degree. The RS658CH0-to-PR-715 spectroradiometer distance was adjusted to produce a measured spot size of approximately 25 mm diameter at the RS658CH0 sphere output port.

The Hoffman RS-658CH0 was measured on two separate occasions, one day apart. The measurements for each day consisted of six separate measurements all at the same lighting of the radiance source. Each of the six measurements consisted of an internal average of three PR-715 measurement cycles. The Hoffman RS-658CH0 was turned on for approximately 30 min to stabilise before the measurements for each day were commenced. The sphere input aperture setting (micrometer) was adjusted to produce a reading of 100% on the power supply display for the "Radiance Level / 100%" dial setting of the power supply, and the "Radiance Level / Lamp Voltage" values were recorded.

The measurements of the Hoffman RS-658CH0 were performed on 2020-February-05 and -06 using PAR QMS procedure PAR-127v0.00.

3.0 Results

All measurements were performed with the optical axis of the PR-715 aligned normal to, and centered on, the face of the Hoffman RS658CH0 sphere output port.

The operating conditions of the Hoffman RS658CH0 are indicated by the three quantities: 1) the sphere input aperture setting (micrometer), 2) the display value for the "Radiance Level / 100%" dial setting of the power supply, and 3) the display value for the "Radiance Level / Lamp Voltage" dial setting of the power supply. The values used for the measurements in this report were:

1) sphere input aperture setting (micrometer) = 0.803″.
2) "Radiance Level / 100%" display value of 100%.
3) "Radiance Level / Lamp Voltage" display value of 15.751 to 15.753 volts.

The average of the 12 PR-715 spectral radiance measurements at the Hoffman RS658CH0 output port is given in Table One.

Electronic versions of this report (PAR-2020-3684.pdf) and data (PAR-2020-3684Data.xls) are also available.[1]

4.0 Measurement Uncertainties

The measurement uncertainties for the calibration are a combination of the uncertainties in the calibration and use of the NRC PR-715 spectroradiometer, and in the operation of the Hoffman RS658CH0. The estimated fractional standard deviations for the measurements are given in Table One. The column 'NRC Spectroradiometer' is the estimated fractional standard deviation in the calibration of the PR-715 for spectral radiance measurements. The column labeled 'Measurement of RS658CH0' is derived from the fractional standard deviation of the mean of the 12 measurements performed upon the RS658CH0, the estimated repeatability of the PR-715, and the estimated spectral radiance uncertainty due to the wavelength uncertainty of the PR-715.

5.0 Traceability

5.1 The NRC values of spectral irradiance are traceable to the SI unit of spectral irradiance (watt•cm^{-2}•nm^{-1}) through various sources:

i. (300 nm to 690 nm), an international comparison of spectral irradiance lamp standards, and
ii. (700 nm to 1600 nm), through measurements using the NRC absolute radiometer (detector).

The NRC working standard lamps of spectral irradiance are calibrated from NRC primary standard lamps of spectral irradiance. The spectral irradiance of these primary lamp standards was determined by comparison with the lamps indicated in i) above, and by direct measurement in ii) using detectors that were calibrated using NRC room temperature absolute radiometers.

5.2 The nonfluorescent reflectance standard (diffuser) was pressed polytetrafluoroethylene (PTFE) powder (1.0±0.1 gm/cm^3) whose absolute spectral radiance factors, $\beta_{45/0}(\lambda)$,

[1] In case of differences between the electronic version and the printed version in this report, the official NRC report data will prevail.

from 380 nm to 1100 nm are traceable to the National Institute of Standards and Technology (NIST) with a relative uncertainty of 0.5% (95% confidence level).

Table One
Spectral Radiance of Hoffman Engineering Spectral Radiance Standard
Model RS-658CH0, s/n 485
Measured normal to the Hoffman RS658CH0 sphere output port, spot size 25 mm diameter.
Sphere input aperture micrometer setting = 0.803″, Radiance Level = 100%
"Radiance Level / Lamp Voltage" display value of 15.751 to 15.753 volts
Unit of $W*sr^{-1}*m^{-2}*nm^{-1}$

The uncertainty values are given as estimated relative standard (k=1) uncertainties. The expanded uncertainties (k=2) are obtained by assuming a normal distribution and multiplying the combined relative standard uncertainty by a coverage factor of k=2.

Wavelength	Spectral Radiance	Relative Standard Uncertainty			Expanded Relative Uncertainty (k=2)
nm	$W*sr^{-1}*m^{-2}*nm^{-1}$	NRC Spectro-radiometer	Measurement of RS658CH0	Combined Quadrature Sum	
380.0	8.202E-03	3.10%	1.04%	3.27%	6.54%
384.0	8.878E-03	3.12%	0.93%	3.26%	6.51%
388.0	9.595E-03	3.08%	0.59%	3.14%	6.28%
392.0	1.031E-02	2.88%	0.49%	2.92%	5.85%
396.0	1.112E-02	2.49%	0.67%	2.58%	5.15%
400.0	1.208E-02	2.10%	0.77%	2.24%	4.48%
404.0	1.304E-02	2.10%	0.66%	2.20%	4.41%
408.0	1.404E-02	2.10%	0.42%	2.14%	4.28%
412.0	1.497E-02	2.09%	0.15%	2.10%	4.20%
416.0	1.597E-02	2.10%	0.46%	2.15%	4.29%
420.0	1.710E-02	2.09%	0.46%	2.14%	4.29%
424.0	1.823E-02	2.09%	0.34%	2.12%	4.24%
428.0	1.941E-02	2.09%	0.25%	2.11%	4.22%
432.0	2.057E-02	2.09%	0.31%	2.12%	4.23%
436.0	2.184E-02	2.10%	0.30%	2.12%	4.24%
440.0	2.312E-02	2.10%	0.24%	2.11%	4.22%
444.0	2.455E-02	2.10%	0.36%	2.13%	4.25%
448.0	2.604E-02	2.09%	0.27%	2.11%	4.23%
452.0	2.748E-02	2.08%	0.21%	2.09%	4.17%
456.0	2.890E-02	2.04%	0.20%	2.05%	4.09%
460.0	3.030E-02	2.00%	0.23%	2.01%	4.03%
464.0	3.178E-02	1.96%	0.28%	1.98%	3.96%
468.0	3.326E-02	1.92%	0.14%	1.93%	3.86%
472.0	3.466E-02	1.88%	0.12%	1.89%	3.78%
476.0	3.616E-02	1.85%	0.19%	1.86%	3.71%
480.0	3.769E-02	1.81%	0.16%	1.82%	3.63%

484.0	3.932E-02	1.77%	0.16%	1.78%	3.56%
488.0	4.098E-02	1.74%	0.13%	1.74%	3.49%
492.0	4.261E-02	1.72%	0.14%	1.73%	3.46%
496.0	4.427E-02	1.72%	0.13%	1.73%	3.45%
500.0	4.588E-02	1.72%	0.09%	1.72%	3.44%
504.0	4.751E-02	1.72%	0.08%	1.72%	3.44%
508.0	4.912E-02	1.72%	0.08%	1.72%	3.44%
512.0	5.067E-02	1.72%	0.07%	1.72%	3.44%
516.0	5.222E-02	1.72%	0.08%	1.72%	3.44%
520.0	5.376E-02	1.72%	0.08%	1.72%	3.44%
524.0	5.541E-02	1.72%	0.08%	1.72%	3.44%
528.0	5.710E-02	1.72%	0.08%	1.72%	3.44%
532.0	5.869E-02	1.72%	0.09%	1.72%	3.44%
536.0	6.022E-02	1.72%	0.11%	1.72%	3.44%
540.0	6.167E-02	1.72%	0.13%	1.72%	3.44%
544.0	6.318E-02	1.72%	0.11%	1.72%	3.44%
548.0	6.477E-02	1.72%	0.13%	1.72%	3.44%
552.0	6.631E-02	1.71%	0.16%	1.72%	3.44%
556.0	6.790E-02	1.72%	0.15%	1.72%	3.45%
560.0	6.948E-02	1.72%	0.16%	1.73%	3.45%
564.0	7.106E-02	1.72%	0.13%	1.72%	3.44%
568.0	7.269E-02	1.72%	0.13%	1.72%	3.44%
572.0	7.427E-02	1.72%	0.12%	1.72%	3.44%
576.0	7.590E-02	1.72%	0.13%	1.72%	3.44%
580.0	7.744E-02	1.72%	0.17%	1.72%	3.45%
584.0	7.896E-02	1.72%	0.16%	1.72%	3.45%
588.0	8.041E-02	1.72%	0.20%	1.73%	3.46%
592.0	8.173E-02	1.72%	0.19%	1.73%	3.46%
596.0	8.306E-02	1.72%	0.18%	1.73%	3.45%
600.0	8.433E-02	1.72%	0.16%	1.72%	3.45%
604.0	8.572E-02	1.72%	0.16%	1.73%	3.45%
608.0	8.698E-02	1.72%	0.17%	1.72%	3.45%
612.0	8.816E-02	1.71%	0.14%	1.72%	3.44%
616.0	8.924E-02	1.71%	0.14%	1.72%	3.44%
620.0	9.035E-02	1.71%	0.13%	1.72%	3.44%
624.0	9.163E-02	1.71%	0.14%	1.72%	3.44%
628.0	9.291E-02	1.71%	0.16%	1.72%	3.44%
632.0	9.410E-02	1.71%	0.13%	1.72%	3.44%
636.0	9.523E-02	1.71%	0.15%	1.72%	3.44%
640.0	9.620E-02	1.71%	0.18%	1.72%	3.45%
644.0	9.719E-02	1.71%	0.14%	1.72%	3.44%

648.0	9.825E-02	1.71%	0.14%	1.72%	3.44%
652.0	9.935E-02	1.71%	0.16%	1.72%	3.44%
656.0	1.005E-01	1.71%	0.19%	1.72%	3.45%
660.0	1.016E-01	1.71%	0.16%	1.72%	3.44%
664.0	1.029E-01	1.71%	0.12%	1.72%	3.44%
668.0	1.042E-01	1.72%	0.14%	1.72%	3.44%
672.0	1.053E-01	1.71%	0.12%	1.72%	3.44%
676.0	1.063E-01	1.72%	0.12%	1.72%	3.44%
680.0	1.072E-01	1.71%	0.16%	1.72%	3.44%
684.0	1.080E-01	1.71%	0.13%	1.72%	3.44%
688.0	1.091E-01	1.71%	0.08%	1.71%	3.43%
692.0	1.103E-01	1.52%	0.07%	1.52%	3.03%
696.0	1.114E-01	1.13%	0.08%	1.14%	2.27%
700.0	1.125E-01	0.77%	0.07%	0.77%	1.55%
704.0	1.136E-01	0.77%	0.07%	0.78%	1.55%
708.0	1.146E-01	0.78%	0.08%	0.78%	1.56%
712.0	1.156E-01	0.77%	0.08%	0.78%	1.55%
716.0	1.166E-01	0.77%	0.08%	0.78%	1.56%
720.0	1.175E-01	0.77%	0.07%	0.77%	1.55%
724.0	1.184E-01	0.78%	0.08%	0.78%	1.56%
728.0	1.194E-01	0.78%	0.09%	0.78%	1.56%
732.0	1.203E-01	0.77%	0.10%	0.78%	1.56%
736.0	1.210E-01	0.77%	0.10%	0.78%	1.56%
740.0	1.217E-01	0.77%	0.07%	0.77%	1.54%
744.0	1.225E-01	0.77%	0.10%	0.78%	1.55%
748.0	1.230E-01	0.77%	0.12%	0.78%	1.56%
752.0	1.237E-01	0.77%	0.10%	0.78%	1.55%
756.0	1.242E-01	0.77%	0.15%	0.78%	1.56%
760.0	1.246E-01	0.77%	0.15%	0.79%	1.58%
764.0	1.252E-01	0.77%	0.10%	0.77%	1.55%
768.0	1.258E-01	0.77%	0.09%	0.77%	1.55%
772.0	1.263E-01	0.77%	0.11%	0.78%	1.55%
776.0	1.267E-01	0.77%	0.13%	0.78%	1.57%
780.0	1.270E-01	0.77%	0.11%	0.78%	1.55%
784.0	1.275E-01	0.78%	0.07%	0.78%	1.57%
788.0	1.280E-01	0.77%	0.12%	0.78%	1.57%
792.0	1.283E-01	0.78%	0.15%	0.79%	1.59%
796.0	1.286E-01	0.78%	0.11%	0.79%	1.58%
800.0	1.289E-01	0.77%	0.13%	0.78%	1.56%
804.0	1.291E-01	0.79%	0.17%	0.81%	1.61%
808.0	1.292E-01	0.80%	0.14%	0.81%	1.62%

812.0	1.295E-01	0.80%	0.13%	0.81%	1.62%
816.0	1.296E-01	0.79%	0.16%	0.81%	1.62%
820.0	1.297E-01	0.80%	0.17%	0.82%	1.64%
824.0	1.298E-01	0.80%	0.15%	0.81%	1.62%
828.0	1.299E-01	0.79%	0.12%	0.80%	1.59%
832.0	1.301E-01	0.80%	0.13%	0.81%	1.62%
836.0	1.301E-01	0.82%	0.14%	0.83%	1.67%
840.0	1.302E-01	0.91%	0.15%	0.92%	1.85%
844.0	1.302E-01	0.84%	0.16%	0.85%	1.71%
848.0	1.302E-01	0.90%	0.14%	0.91%	1.81%
852.0	1.302E-01	0.90%	0.20%	0.92%	1.85%
856.0	1.300E-01	0.99%	0.16%	1.00%	2.01%
860.0	1.301E-01	1.13%	0.14%	1.14%	2.28%
864.0	1.298E-01	1.16%	0.26%	1.19%	2.38%
868.0	1.295E-01	1.13%	0.16%	1.14%	2.28%
872.0	1.296E-01	1.32%	0.12%	1.32%	2.65%
876.0	1.295E-01	1.23%	0.19%	1.25%	2.49%
880.0	1.293E-01	1.21%	0.16%	1.22%	2.45%
884.0	1.292E-01	1.06%	0.16%	1.07%	2.13%
888.0	1.290E-01	1.01%	0.17%	1.02%	2.05%
892.0	1.289E-01	0.96%	0.15%	0.97%	1.94%
896.0	1.287E-01	0.98%	0.18%	1.00%	1.99%
900.0	1.285E-01	0.98%	0.13%	0.99%	1.98%
904.0	1.284E-01	0.88%	0.16%	0.90%	1.79%
908.0	1.280E-01	0.91%	0.25%	0.94%	1.89%
912.0	1.276E-01	0.83%	0.17%	0.85%	1.69%
916.0	1.275E-01	0.84%	0.15%	0.86%	1.71%
920.0	1.272E-01	0.85%	0.16%	0.87%	1.73%
924.0	1.271E-01	0.83%	0.14%	0.84%	1.68%
928.0	1.267E-01	0.82%	0.19%	0.84%	1.69%
932.0	1.264E-01	0.83%	0.17%	0.85%	1.70%
936.0	1.262E-01	0.83%	0.17%	0.84%	1.69%
940.0	1.261E-01	0.82%	0.24%	0.85%	1.70%
944.0	1.254E-01	0.80%	0.31%	0.86%	1.71%
948.0	1.250E-01	0.80%	0.13%	0.81%	1.62%
952.0	1.248E-01	0.80%	0.22%	0.83%	1.65%
956.0	1.242E-01	0.78%	0.34%	0.85%	1.70%
960.0	1.236E-01	0.80%	0.22%	0.83%	1.66%
964.0	1.236E-01	0.80%	0.18%	0.82%	1.64%
968.0	1.232E-01	0.81%	0.27%	0.86%	1.72%
972.0	1.227E-01	0.79%	0.22%	0.82%	1.63%

976.0	1.223E-01	0.79%	0.31%	0.85%	1.69%
980.0	1.216E-01	0.78%	0.35%	0.86%	1.71%
984.0	1.222E-01	0.80%	0.37%	0.88%	1.76%
988.0	1.215E-01	0.79%	0.29%	0.84%	1.68%
992.0	1.216E-01	0.80%	0.33%	0.86%	1.73%
996.0	1.208E-01	0.80%	0.31%	0.86%	1.72%
1000.0	1.207E-01	0.80%	0.32%	0.86%	1.72%
1004.0	1.200E-01	0.83%	0.36%	0.90%	1.80%
1008.0	1.200E-01	0.82%	0.30%	0.87%	1.73%
1012.0	1.195E-01	0.84%	0.38%	0.92%	1.84%
1016.0	1.190E-01	0.81%	0.27%	0.85%	1.71%
1020.0	1.193E-01	0.84%	0.45%	0.95%	1.90%
1024.0	1.191E-01	0.83%	0.93%	1.25%	2.50%
1028.0	1.168E-01	0.89%	1.12%	1.43%	2.86%
1032.0	1.186E-01	0.89%	0.85%	1.24%	2.47%
1036.0	1.177E-01	0.88%	0.69%	1.12%	2.25%
1040.0	1.181E-01	0.90%	0.82%	1.22%	2.43%
1044.0	1.187E-01	1.01%	0.85%	1.32%	2.63%
1048.0	1.177E-01	0.94%	1.06%	1.42%	2.83%
1052.0	1.166E-01	0.99%	1.32%	1.65%	3.30%
1056.0	1.198E-01	1.08%	1.62%	1.95%	3.89%
1060.0	1.201E-01	0.93%	1.01%	1.38%	2.76%
1064.0	1.172E-01	1.09%	1.45%	1.81%	3.63%
1068.0	1.174E-01	1.37%	1.56%	2.07%	4.15%

Appendix D: Data Calibration Procedure

Setup

1. Setup the Integrating sphere beneath the IS platform mounted on the IS Rack in an upward viewing position mounted on the lab-jack which in turn is mounted on the XY translation stages with the long axis (X) aligned perpendicular to the line image direction the imaging spectrometer are to be mounted in. Lab-jack should be fully retracted (minimum height) at this time.
2. Install the imaging spectrometer under test in a nadir (downward) viewing position on the IS platform with lens protruding though the platform viewing hole. Bolts are to be use to secure the CASI and WISE sensor heads to the platform. Use the rotational control on the platform support (yellow apparatus) to ensure that the sensor is nadir viewing.
3. Set up the Hr1024i on the tripod mounted arm with the bottom of the lens at approximately the same height as the imaging spectrometer lens. Use the 3-axis trip head to ensure that the HR1024i is in a nadir viewing position.
4. Swing the tripod arm so that the HR1024i abuts against the front edge of the platform while adjusting the position of the fore-optics in the Y axis so that it is aligned with the centre of the imaging spectrometer FOV.
5. Turn on the HR1024 making measurements in order to monitor the VNIR temperature as it stabilises. Ideally the measurements should be made at 36.6 °C, the temperature at which the HR1024i calibration data was acquired at SVC. This may take 2 hours or more. Steps 6 through 13 below can be performed while the HR1024i stabilization is occurring.
6. Turn on the imaging spectrometer under investigation. Provide a minimum of 10 minutes before initiating any measurements.
7. Start the imaging spectrometer software and set the configuration to full (288 channels) with an integration time similar to that used during airborne acquisitions.
8. Turn on the integrating sphere. Stabilization will not take long (a couple of minutes maximum) and will be ensured by monitoring the integrating sphere monitoring
9. Once the integrating sphere monitoring photodiode stabilizes, turn off lab lights and any other illumination sources in the lab, and adjust the integrating sphere Vernier to provide a readout of 100.0%.
10. Note the setting of the Vernier caliper to ensure that it remained unchanged from that used during the NRC integrating sphere calibration.
11. Determine the X stage position that aligns:
    - The centre of the HR1024i FOV with the centre of the integrating sphere exit port (use the HR1024i locating laser to assist with this);
    - The centre of the imaging spectrometer with the centre of the integrating sphere exit port (providing the widest image of the port when scanned).
12. Measure and record the lens-to port distance for both the:

- HR1024i;
- Imaging spectrometer under test.

13. Position the integrating sphere below the HR1024i.

Absolute and Relative Validation Assessment Data Acquisition Process

14. Darken lab.
15. Reset the sphere Verner to provide a 100.0% on the monitoring photo-diode.
16. Take a HR1024i reference scan immediately followed by a target scan.
17. Position the integrating sphere below the imaging spectrometer.
18. Start image acquisition.
19. Record the integrating sphere photodiode monitor readout.
20. Once the pre-image data has been acquired, ensure that at least 512 scan lines of the integrating port are acquired (1 frame) and then stop data acquisition.
21. Record raw image file acquisition name.
22. Adjust the Y-Axis to position:
    - -26000000 (extreme limit of the Y-stage) for the CASI and WISE imaging spectrometers;
    - -20000000 for the narrower FOV μCASI.
23. Raise the integrating sphere using the control knob on the lab-jack until only 2/3rd of the port image remain within the display.
24. Start data acquisition.
25. Monitor and record the integrating sphere photodiode monitor readout periodically during the following step.
26. Once imagery of the integrating sphere port filling at least one page is viewed on display, adjust the Y-axis by step of:
    - -625000 for the CASI and WISE;
    - -500000 for the μCASI.
27. Stop data acquisition.
28. Record raw image file acquisition name.
29. Return Y-Axis to position 0.
30. Lower lab-jack to original position.
31. Adjust the X-Axis back to the position the integrating sphere beneath the HR1024i.
32. Record the integrating sphere photodiode monitor readout (if the setting has changed from 100.0%, do not adjust, simply record the new value).
33. Take a HR1024i target scan.
34. Perform a preliminary validity check of acquired data by ensuring that the ratio of the final target scan to the initial reference scan approximates 1.0 across the entire spectral range ensuring that the integrating sphere remained stable. If the ratio does not approximate 1.0, consider repeating steps 13 through 34.
35. Return the X-Y-stage to home position (0, 0).

Linearity Validation Assessment Data Acquisition Process

36. Position sphere below instrument under test (spectroradiometer, WISE, CASI, μCASI).
37. Turn lights off.
38. For each setting/measurement level, set sphere output using the Vernier control to provide the following values on the monitoring photo-diode:
    - Recommended settings used for this first attempt: 130.0%, 120,0%, 110.0%, 100.0%, 75.0%, 50.00%, 25.00%, 10.00%, 5.000%, 1.000%, 0.500%, 0.100%, 0.050%, 0.010%, 0.005%, 0.000%
    - Note that the precision provided above, are those achievable on the sphere controller when properly using the precision control adjustment.
    - Note that for the μCASI, the system saturates over a portion of the spectral range at setting of 100.0% and above; setting above 100.0% can be ignored.
39. Acquire data:
    - For the spectroradiometer, a single reference scan followed by a single target scan at each sphere setting levels.
    - For the 3 HSI instruments, all data can be acquired in a single file in order to reduce data acquisition time, with a full frame of imagery acquired at each radiance level once it is achieved.

Shut down

40. Turn on lab lights.
41. Close software programs and turn off equipment.
42. Install lens covers.

NRC.CANADA.CA • INFO@NRC-CNRC.GC.CA • 877-672-2672 •